THE AMYOTROPHIC LATERAL SCLEROSIS 8 MUTANT VAPB-P56S CAUSES A NUCLEAR ENVELOPE AND NUCLEAR PORE DEFECT

Antonious Chalhoub

Thesis Supervisor
Dr. Johnny K. Ngsee

This Thesis is Submitted as a Partial Fulfilment of the M.Sc. Program in Neuroscience

August 14, 2012

Faculty of Medicine
Department of Cellular & Molecular Medicine
Neuroscience Program
University of Ottawa
Ottawa, Ontario, Canada

ABSTRACT

A P56S mutation in the VAPB MSP domain is linked to adult-onset amyotrophic lateral sclerosis 8. The objective of this study is to characterize the functional role of VAPB in transport of NE and NPC proteins from the ER to the NE. Over-expression of VAPB-P56S blocked the transport of nucleoporins (Nups) and NE proteins, resulting in their sequestration in dilated cytoplasmic membranes. Simultaneous overexpression of the FFAT motif (two phenylalanines in an acidic track) antagonizes mutant VAPB effects and restores transport to the NE. VAPB function is required for transport to the NE because knockdown of endogenous VAPB recapitulates this phenotype. Moreover, the compartment in which Nups and NE proteins are sequestered and retained was identified as ER-Golgi intermediate compartment (ERGIC). Moreover, a defect in the transport of NE and NPC proteins attenuates nucleocytoplasmic shuttling of the glucocorticoid receptor (GR). Further, VAPB-P56S which is only soluble in SDS was solubilized in the Triton-X-100 fraction similar to VAPB-WT upon co-transfection with the FFAT motif suggesting that FFAT interacts with the insoluble VAPB-P56S protein changing its biophysical properties.

TABLE OF CONTENTS

LIST OF FIGURES

LIST OF ABBREVIATIONS

(ALS)	Amyotrophic Lateral Sclerosis
(BSA)	Bovine Serum Albumin
(CCD)	Coiled-Coil Domain
(cDNA)	Complimentary Deoxyribonucleic Acid
(CHO)	Chinese Hamster Ovary
(CNS)	Central Nervous System
(DIM)	Dimerization
(EM)	Electron Microscopy
(EPSPs)	Excitatory Postsynaptic Potentials
(ER)	Endoplasmic Reticulum
(ERG30)	Endoplasmic Reticulum and Golgi 30-kDa protein
(ERGIC)	ER-Golgi Intermediate Compartment
(FALS)	Familial ALS
(FFAT)	Two phenylalanines in an acidic tract
(GFP)	Green Fluorescent Protein
(MEM)	Minimum Essential Medium
(MSP)	Major Sperm Protein
(NE)	Nuclear Envelope
(NLS)	Nuclear Localization Sequence
(NPCs)	Nuclear Pore Complexes
(Nups)	Nucleoporins
(OHD)	OSBP Homology Domain
(ORD)	OSBP-Related ligand-binding Domain
(ORPs)	OSBP-Related Proteins
(OSBP)	Oxysterol-Binding Proteins
(PH)	Pleckstrin homology
(PM)	Plasma Membrane
(PNS)	Perinuclear Space
(rdgB)	Retinal Degeneration Type B protein
(RFP)	Red Fluorescent Protein
(SALS)	Sporadic ALS
(SCS2)	Suppressor of Choline Sensitivity 2
(SNARE)	Soluble *N*-ethylmaleimide-sensitive factor attachment protein Receptor
(TMD)	Transmembrane domain
(VAMP)	Vesicle-Associated-Membrane-Protein
(VAP33)	VAP of 33 kDa
(VAPB)	Vesicle-Associated-membrane protein-associated protein B

ACKNOWLEDGEMENTS

Finding your passion comes with many obstacles. You initially set a goal and then work to achieve it. Along the way, experiences make you change your goal or try harder to obtain it. In my Master's I have learnt that even though you may not have obtained your final goal there is great knowledge gained if you appreciate your situation, your surroundings and the people in your life during that moment. Embarking on a Master's of neuroscience is not an easy road, and along the way I have encountered doubt about what I was doing. However, by appreciating the people that gambled on my success and the community that has funded my research, I see how privileged I am. Today, through a publication and the collaboration of myself and my lab partners, we were able to make a change in the way researchers will examine ALS8.

I appreciate the guidance and patience of my supervisor, Dr. Johnny K. Ngsee. His support and strength has helped me get through the program. I am lucky to have been given the privilege to work with Dr. Ngsee. Initially, I was mentored by Duvinh Tran a Master's graduate. He is extremely educated in his field and was always there when needed. Kalina Abrol, was my emotional support during the program and she always pushed me to do better. By working with Angie Darbyson, a Master's student, many of my doubts as to why I was doing ALS research were answered. She suffered from the loss of a family member affected by ALS, and through Angie I remembered what the research was about. Angie has a great amount of determination and love in her research and I am lucky to have met her. Further, I thank the members of my advisory committee for their guidance on my project: Dr. Antonio Colavita and Dr. Jean-Claude Beique. Lastly, I thank Dr. Thompson for helping me on the confocal microscope.

I thank everyone that has been there during the past years and I have grown to admire their love for the field of neuroscience.

INTRODUCTION

Amyotrophic Lateral Sclerosis

Amyotrophic lateral sclerosis (ALS) is a neurological disorder defined by the progressive loss of upper and lower motor neurons in the cerebral cortex, brainstem and spinal cord. The loss of motor neurons in these regions results in weakness, muscular atrophy and loss of voluntary movement. Further, patients exhibit difficulty in speech and swallowing eventually leading to full paralysis. Typically, death is followed approximately 1-5 years after a patient is diagnosed due to respiratory failure (Cozzolino et al., 2008). A devastating property of patients affected by ALS is that they tend to exhibit full cognitive functions allowing the patient to be fully aware of their deterioration and loss of their voluntary movement (Cozzolino et al., 2008). The average age of disease onset is 50 years of age (Cozzolino et al., 2008) with an incidence of 1-2 persons out of 100,000 and prevalence of 4-6 persons out of 100,000 (Kanekura et al., 2009; Cozzolino et al., 2008). Incidences of sporadic ALS (SALS) are 90-95% and familial ALS (FALS) cases make up 5-10% (Shaw, 2005). Research has shown that whether the disease is SALS or FALS, the disease is indistinguishable which allows researchers to apply current therapeutic techniques to a wide spectrum of ALS cases.

Amyotrophic Lateral Sclerosis 8 (ALS8)

ALS8 is a late-onset adult neurodegenerative disorder manifested as a movement disorder. The progressive loss of neurons and the degeneration of their synaptic connections is a common characteristic of neurodegenerative disease (Meyer and Quenezer, 2005). Specifically, if neurodegeneration of upper motor neurons and lower motor neurons occurs then the cardinal clinical features become evident in ALS8 patients. The cardinal features are as follows:

weakness, muscular atrophy, loss of voluntary muscle movement and paralysis (Boillee et al., 2006). There are currently eleven types of familial ALS and familial ALS8 is caused by a mutation in the Vesicle-Associated Membrane Protein (VAMP)-associated protein B (VAPB) gene (Nishimura et al., 2004). The VAPB gene encodes a Type II integral membrane protein ubiquitously expressed in the CNS, and abundant in motor neurons (Teuling et al., 2007). Interestingly, VAPB was found to be expressed throughout the CNS in the olfactory bulb, cortex, mesencephelon, hippocampus, cerebellum, medulla oblongata and the spinal cord and yet the genetic P56S mutation in the conserved major sperm protein domain of VAPB causing ALS8 specifically results in motor neuron degeneration (Teuling et al., 2007). Further, VAPB was expressed in the kidney, heart, skeletal muscle, liver, spleen and lung (Teuling et al., 2007). Since VAPB was found to be abundant in motor neurons, a closer examination revealed that VAPB in neurons was concentrated to the soma and proximal dendrites (Teuling et al., 2007). The specificity to motor neuronal death in VAPB-P56S is not well understood; however, studies have shown that the mutation in VAPB forms cytosolic aggregates (Nishimura et al., 2004). Research has been currently emphasizing on the functional deficits that are caused by the P56S aggregates in order to explain the susceptibility to motor neurons.

It has been shown that VAPB-P56S induces a change in ER morphology and leads to a collapse of the ER microtubules resulting in cytoplasmic aggregates (Prosser et al., 2008). Since motor neurons are large cells and have extremely complex morphologies, the selective vulnerability of motor neurons could be due to their great need of ER cellular processes (Boillee et al., 2006). Interestingly, motor neurons have been shown to have an extensive ER network and VAPB is localized to the ER. Taken together, motor neurons may be selectively damaged due to the greater size of their ER, thus a greater abundance of the VAPB protein.

A hallmark study towards understanding ALS produced by Nishimura in 2004 identified the locus for an atypical form of ALS now known as ALS8. The locus was mapped to chromosome 20q13.3 for vesicle-associated-membrane protein-associated protein B (VAPB) (Nishimura et al., 2004). In 2005, a study identified seven families of Portuguese-Brazilian ancestry and one family of African-Brazilian ancestry compromising more than 1,500 individuals and from those families 200 individuals suffered from ALS symptoms (Nishimura et al., 2005). Genetic analysis of the family pedigree identified a common cytosine to thymine substitution at position 166 of the open reading frame (Nishimura et al., 2005). This resulted in substitution of the proline residue at position 56 to serine (P56S) (Nishimura et al., 2005).

Structure of VAPB

VAPs are ER-resident proteins initially discovered due to their interaction with v-SNARE VAMP2 (Skehel et al., 1995). The first VAP was identified in *Aplysia californica* as VAP of 33kDA (VAP33) (Skehel et al., 1995). In humans, there are only two VAP genes encoding for the VAP proteins VAPA, VAPB and the VAPB spliced variant VAPC. VAPA and VAPB are similar isoforms sharing 63% identical amino acids (Nishimura et al., 2004). Both VAPA and VAPB contain an N-terminal major-sperm protein (MSP) domain, a central coiled-coil region, and a C-terminal transmembrane domain (Nishimura et al., 1999) (Fig. 1 A and B). VAPC lacks the coiled-coil and transmembrane regions. Although these VAPs are grouped in the same family, they hold unique properties. VAPA gene is located on chromosome 18 and encodes a 249 amino acids long protein with a predicted molecular mass of 27.3kDa (Nishimura et al., 1999). VAPB gene is located on chromosome 20 and encodes a 243 amino acids long protein with a predicted molecular mass of 27 kDa (Nishimura et al., 1999) (Fig. 1B). VAPC is the same gene as VAPB but is an mRNA splice variant that leads to a truncated protein (Kukihara et al., 2009). The major

sperm protein (MSP) domain of VAPB consists of 150 amino acids organized into a seven-stranded immunoglobin-like-β-sandwich with S-type topology (Baker et al., 2002). The MSP domain is essential for the VAP-FFAT interaction because the MSP domain is the region that directly interacts with the FFAT motif of lipid binding proteins (Loewen and Levine, 2005). The coil-coiled domain is comprised of 40 amino acids and is suggested to function in protein-protein interaction (Hamamoto et al., 2005). VAPB's transmembrane domain acts as an anchor anchoring VAP to the ER membrane which plays a crucial role in VAPBs ability to form homo- and heterodimers via its dimerization motif (GxxxG) (Amarilio et al., 2005). VAPA and VAPB localize to the ER and research suggests their primary function is within this compartment (Soussan et al., 1999) involved in the early or late secretory pathway of protein transport from the ER.

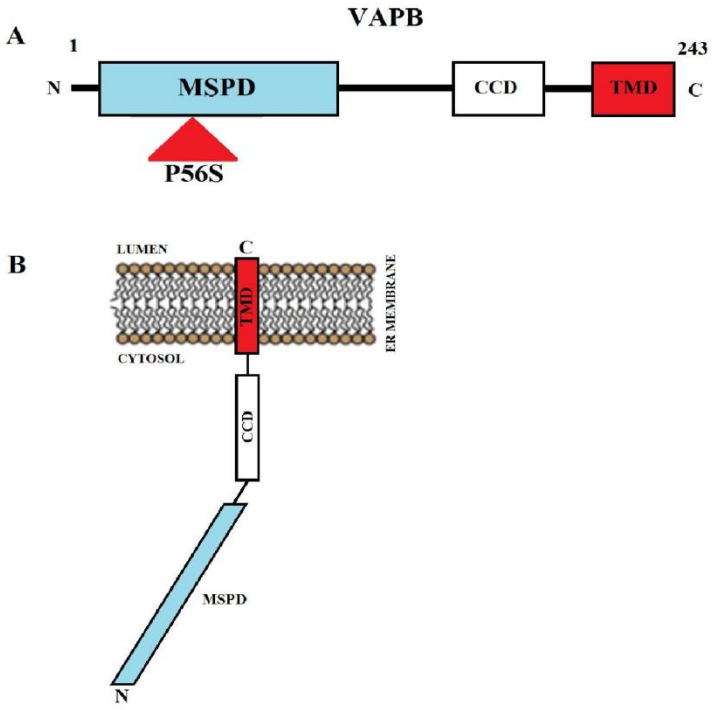

Figure 1. VAPB Structure. (A) VAPB structure illustrating three conserved domains: The N-terminal major sperm domain (MSPD), a middle coil-coiled domain (CCD), and the C-terminal transmembrane domain (TMD). The P56S red arrow in VAPB indicates the site of the missense mutation in ALS8. (B) VAPB orientation in the ER membrane. VAPB is a type II integral membrane protein with the C-terminal TMD anchored to the ER membrane and the N-terminal MSPD towards the cytosol.

The Consequences of VAPB-P56S

The P56S mutation in ALS8 resides in the conserved MSP domain of VAPB (Nishimura et al., 2004). The hallmark of the P56S missense substitution is ER membrane aggregates that are resistant to degradation (Kanekura et al., 2006; Nishimura et al., 2004; Teuling et al., 2007). Studies have shown that the mutant form of VAPB has the ability to recruit wild-type VAPA and VAPB into insoluble aggregates leading to a loss of function of the wild-type protein (Teuling et al., 2007). Since VAPB has the ability to form dimers, it is possible that this recruitment could be due to a mutated form of VAPB forming dimers with wild-type VAPB. In addition, this recruitment could also be due to the aggregation of the MSP domain simply aggregating nearby wild-type VAPB. Although, it is not clear which mechanism is responsible for mediating neuronal cell death, aggregation and recruitment of the wild-type form of VAPB by the mutant form of VAPB could additively over time trigger cell death.

A mutation in copper-zinc superoxide dismutase (SOD1) has been linked to a form of familial ALS known as ALS1. This form of ALS is the most common genetic cause of ALS (Tsuda et al., 1994). A mouse model of SOD1 for ALS1 has shown that both VAPA and VAPB levels were down-regulated (Teuling et al., 2007). What this study suggests is that ALS1 may also cause effects similar to ALS8. The loss of VAP from SOD1 mice in ALS1 and the loss of VAP in VAP-P56S transfected cells in ALS8 can be a leading factor in the pathogenesis of the disease.

Collectively, studies examining VAPB-P56S in cellular models have consistently shown mutant VAPB to be aggregates prone and recruiting endogenous VAPB to insoluble aggregates resulting in a dominant negative effect (Teuling et al., 2007). Animal models such as *Drosophila melanogaster* and transgenic mice have been able to display these aggregates. Unfortunately, at the present time there is no confirmation that these aggregates are present in human tissue;

therefore, most of the information gathered about these aggregates and the loss of proper function due to VAPB-P56S mutation has to be generalized with existing models. In a model utilizing *Drosophila melanogaster* the aggregates seen in cells have been reproduced (Chai et al., 2008). The transgenic expression of mutant dVAPP56S in *Drosophila* reproduced these aggregate structures (Chai et al., 2008). Further, transgenic mice expressing the human P56S mutation of VAPB also reproduced these cytoplasmic aggregates (Tudor et al., 2010).

The Highly Conserved MSP Domain of VAPB

The MSP domain of VAPB is homologous to the major sperm protein of the nematodes *A. suum and Caenorhabditis elegans* (Skehel et al., 2000). The crystal structure of VAPBs MSP domain confirms that the MSP domain consists of 150 amino acids organized into a seven-stranded immunoglobin-like-β-sandwich with S-type topology (Baker et al., 2002). Uncovering the crystal structure revealed that the P56S mutation of VAPB is in the MSP domain of VAPB at a kink within the extended β-sheet (Loewen and Levine, 2005). The S-shape loop is maintained by the proline residue at codon 56 which connects the d1 and d2 strands within the MSP domain resulting in an S-shape pattern (Nishimura et al., 2004). The proline stabilizes the S-shape loop by holding it in a less energetically favourable *cis*-peptide bond conformation (Teuling et al., 2007). The MSP domain has hydrophobic core residues, and the S-shape loop formed by the proline residue shields these core residues (Teuling et al., 2007). Since VAPB-P56S forms insoluble cytoplasmic aggregates (Kanekura et al., 2006), it is suggested that upon substitution of proline to a serine residue the S-shape loop destabilizes into a more energetically favourable *trans*-peptide bond conformation (Teuling et al., 2007).This change in protein conformation exposes the hydrophobic core residues and formed aggregates may be the result of

accumulating neighbouring mutant VAPB proteins attempting to shield the exposed hydrophobic core residues (Teuling et al., 2007).

In 2006 it was found that the loss of the proline residue is the main cause of the formed aggregates and change in ER morphology (Kanekura et al., 2006). VAPB was mutated by substituting the proline residue with amino acids such as alanine, lysine or aspartic acid. In all cases VAPB increased insolubility similar to the P56S mutation in ALS8 (Kanekura et al., 2006). Proline's ability to maintain the S-shape loop in the MSP domain shields the hydrophobic core residues and maintains the proper protein conformation of VAPB. The loss of the proline residue results in the mis-folding of VAPB and *In vitro* studies have shown that over-expression of VAPB-P56S consistently produces polyubiquitinated, detergent-insoluble, cytoplasmic aggregates (Kanekura et al., 2006). It is certain that the mutation in VAPB prevents the proper folding of the protein interfering with its function (Kanekura et al., 2006).

Possible VAP function

Earlier studies have addressed the possible functions of VAPs. Initially, VAPA was identified as VAP of 33 kDa or VAP33 (Nishimura et al., 2004). Although VAPA holds unique properties and functions, VAPA and VAPBs sequence and protein structure similarity may suggest that VAPA function may be applicable to VAPB (Nishimura et al., 2004). Research has implemented VAPA and VAPB in intracellular trafficking, the unfolded protein response (UPR) and with phospholipid metabolism. A disruption in one of these pathways may explain why motor neurons are targeted in ALS8 and may define the mechanism by which the disease is caused.

Intracellular Trafficking

The transport of proteins between organelle compartments in the protein secretory pathway requires a great deal of proteins to mediate vesicle budding and fusion events. For the survival of the cell, this pathway must be followed and disruption to this pathway can diminish cellular functions. Currently, VAP has been linked to intracellular trafficking; however, the specific role of VAPB is still in debate and is not yet fully understood. Further, the negative effects caused by VAPB-P56S cytoplasmic aggregates are also still underway. The protein secretory pathway consists of the early and late secretory pathways (Fig. 2). Specifically, VAPB is implicated in the early secretory pathway. Proteins are synthesized at the endoplasmic reticulum (ER); subsequently, the proteins are shuttled to the ER-Golgi intermediate compartment (ERGIC) from which proteins are transported to the *cis*-Golgi network (CGN). Following, proteins are transported to the *trans*-Golgi network (TGN). At the TGN the proteins are sorted and transported to their final localization. The pathway described illustrates the anterograde transport route from the initial synthesis of proteins to their final localization. Since the ER is the site of lipid production, anterograde transport is the main route for synthesized proteins and lipids (Prosser, 2008). However, this pathway also consists of retrograde transport located within the Golgi complex – between the CGN and TGN – and from the Golgi network back to the ER (Prosser, 2008).

Research suggests that VAPB is implicated in ER to Golgi protein trafficking. In 1999, the ER and Golgi 30-kDa protein (ERG30), known as VAPB, was implicated in protein transport between the ER and Golgi (Soussan et al., 1999). They showed that the use of an ERG30 antibody *in vitro* resulted in COPI-coated vesicles accumulation at the Golgi complex (Soussan et al., 1999) linking VAPB to the early secretory pathway between the ER and the Golgi. There are anterograde and retrograde pathways in the protein secretory system. COPI-coatomers are involved in the

retrograde transport of proteins from the *cis*-Golgi to the ER (Soussan et al., 1999). The accumulation of COPI vesicles linked VAPB with protein retrograde transport between the ER and Golgi. Thus, VAPB is likely involved in intracellular trafficking of proteins in the early secretory pathway between the ER and the Golgi complex. In the current study, an objective is to understand how VAPB-P56S-induced disruption of protein trafficking between the ER and Golgi may lead to the pathogenesis of ALS8.

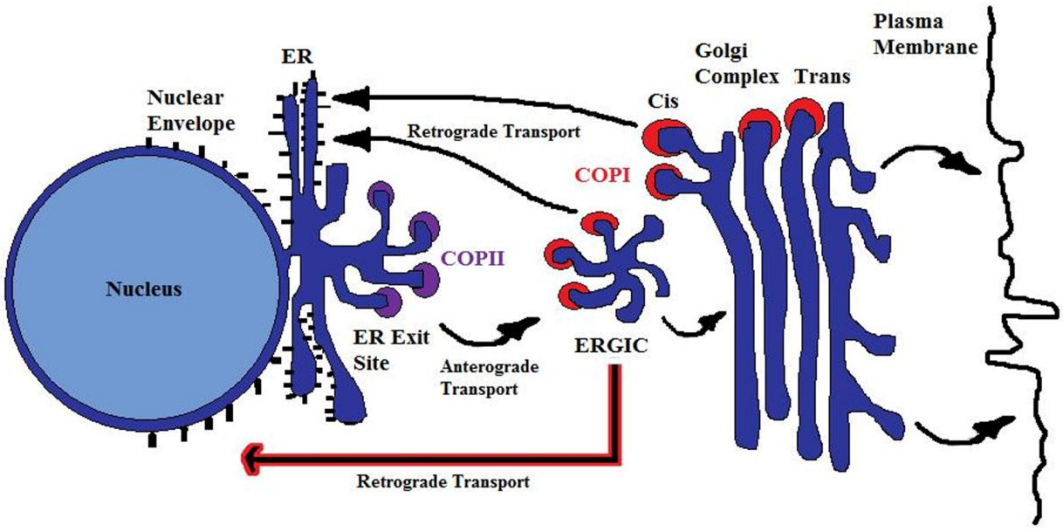

Figure 2. The Secretory Pathway. Proteins are synthesized at the endoplasmic reticulum (ER); subsequently, the proteins are shuttled to the ER-Golgi intermediate compartment (ERGIC) from which proteins are transported to the cis-Golgi network (CGN). Following, proteins are transported to the trans-Golgi network (TGN). At the TGN the proteins are sorted and transported to their final localization, for instance the plasma membrane. The pathway just described illustrates anterograde transport from the initial synthesis of proteins to their final localization via COPII vesicles. Anterograde transport is the main route for synthesized proteins and lipids. However, this pathway also consists of retrograde transport via COPI vesicles within the Golgi complex between the CGN and TGN, from the Golgi network back to the ER and from the ERGIC back to the ER.

Phospholipid Metabolism

The MSP domain of VAPs directly interacts with the FFAT motif of lipid binding proteins. The FFAT motif, two phenylalanines in an acidic tract, was found to be the domain for interaction between FFAT containing proteins and VAPs (Loewen et al., 2003). The FFAT motif has seven amino acids with the consensus sequence EFFDAxE (Kaiser et al., 2005) (Fig. 3 A). Upon binding of VAPs MSP domain to FFAT-motif containing proteins, lipid binding or transfer proteins are recruited to the ER membrane to regulate lipid composition at the ER membrane (Lev et al., 2008; Prosser et al., 2008). Presently, how mutant VAPB affects binding of FFAT with VAP is not fully understood.

Lipid Binding or Transfer Protein Function

Prior to ER membrane recruitment, FFAT motif-containing lipid binding or transfer proteins are localized to the cytosol (Perry and Ridgway, 2006).The cytosol is an aqueous environment with numerous hydrophobic lipids molecules. Lipid binding or transfer proteins function by solubilizing the hydrophobic lipids as they transport through the cytoplasm (Loewen et al., 2003). Arrival at the target membrane induces the FFAT motif-containing lipid binding or transfer proteins to bind to MSP domain of VAP and releases the lipids from lipid binding or transfer proteins to insert them into the membrane (Olkkonen and Levine, 2004). This process regulates the lipid composition at the ER membrane.

Lipid Binding or Transfer Protein Families

VAPs interact with FFAT motif –containing proteins involved in synthesis, transport and metabolism of lipids. Oxysterol-binding proteins (OSBP) contain the FFAT sequence and are cytosolic receptors that bind to oxysterols such as 25-hydrocholoesterol (Wyles et al., 2002). OSBP-related proteins (ORP) are also FFAT motif containing lipid binding proteins consisting of

ORP1L, ORP2, ORP3, ORP4L, ORP6, ORP7, and ORP9. ORPs and OSBP sharer the same OSBP-related ligand-binding domain (ORD) yet differ by protein sequence (Olkkonen et al., 2006). Retinal degeneration type B proteins (rdgB) are also FFAT motif lipid binding proteins consisting of Nir1, Nir2, and Nir3 (Olkkonen and Levine, 2004). This group is involved in membrane trafficking and phospholipid metabolism (Amarilio et al., 2005).

Initial Characterization of the VAP-FFAT interaction

Lipid binding or transfer proteins facilitate intracellular lipid trafficking. To effectively execute their function, lipid binding or transfer proteins must be guided to specific target membranes. The initial finding illustrating the VAP-FFAT interaction was executed in *Saccharomyces cerevisiae* (Loewen et al., 2003) where the FFAT motif acted as a membrane-targeting signal directing proteins to the surface of the ER to bind with VAP (Loewen et al., 2003). Further, the FFAT-motif is found in Opi1p, a transcriptional repressor of genes involved in phospholipid synthesis in yeast (Loewen et al., 2003). Opi1 directly interacts by its FFAT motif with the MSP domain of SCS2, the yeast homologue of VAP, in order to target the ER (Loewen et al., 2003). Upon binding of Opi1 FFAT-motif to SCS2 MSP domain, Opi1 was retained in the cytoplasm preventing Opi1s translocation to the nucleus in order to enhance the transcription of lipid-synthesizing genes (Brickner and Walter, 2004). Thus, binding to VAP is executed by FFAT motif containing proteins to promote the synthesis of new ER membranes and to regulate lipid composition. A disruption in this process can lead to a collapse in ER morphology due to unregulated lipid composition at the ER (Prosser et al., 2008).

Crystallography of the VAP-FFAT Interaction

In 2005, the VAP-FFAT interaction was clarified by crystallography (Kaiser et al., 2005). The crystal structure resolved that the VAPA-FFAT interaction occurs by a 2:2 complex (Fig. 3 B). The MSP domains of the two VAP proteins would each consist of a bound FFAT motif (Kaiser et al., 2005). Further, the residues of VAPA-MSP domain crucial for binding FFAT-containing proteins were resolved. In FFAT containing proteins, the phenylalanine at the 476 residue binds to VAPAs-MSP domain at residue Met89. Binding occurs in a hydrophobic pocket of VAPAs-MSP domain created by aliphatic side chains: Lys45, Thr47, Ly87, and Lys118 (Kaiser et al., 2005).

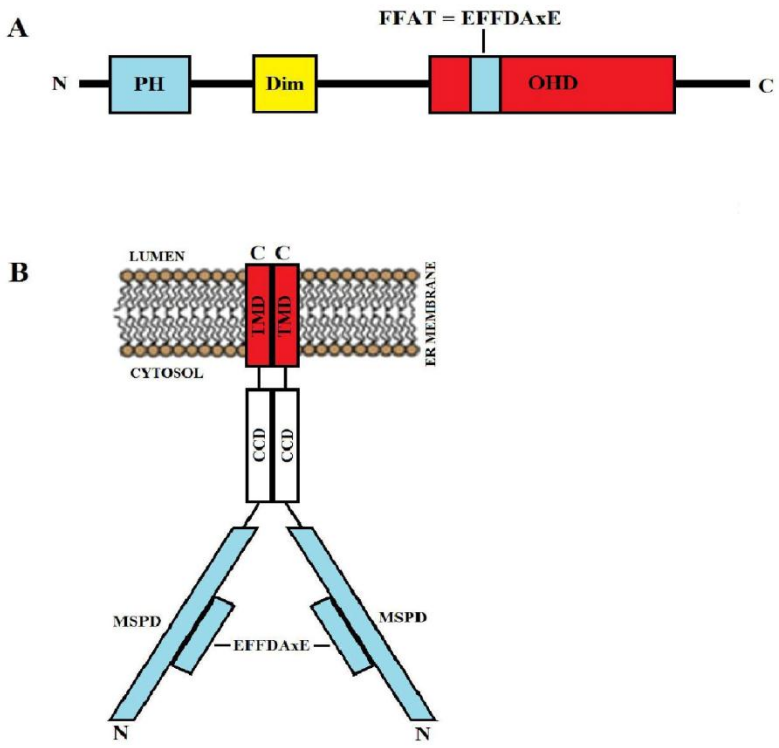

Figure 3. OSBP Structure and VAPB and FFAT interaction. (A) The OSBP structure illustrating the conserved domains: pleckstrin homology (PH) domain spanning residues 91-182, a dimerization (DIM) domain spanning residues 261-296, and a OSBP homology domain (OHD) spanning 417-772. The FFAT motif cloned spanned 347-468. (B) An illustration of the VAPB-FFAT interaction which occurs by a 2:2 complex.

Consequences of Defective VAP-FFAT Binding

Brunger's group (2005) mutated the key residues of the VAP-FFAT interaction in the hydrophobic pocket and aliphatic side chains of Scs2p, VAP homologue in yeast, K87D/M89D (Kaiser et al., 2005).This mutation disrupted the interaction between Scs2 and the FFAT containing protein Opi1; thus, blocking the function of Scs2p (Kaiser et al., 2005). The defective binding between FFAT containing proteins and VAP has shown to produce severe abnormalities to ER morphology and cellular processes (Prosser et al., 2008; Kaiser et al., 2005). Upon expressing the K87D/M89D mutation in COS7 cells, Brunger's group showed severely altered ER morphology (Kaiser et al., 2005). Untreated cells exhibited normal reticular ER pattern whereas over-expression of VAPA K87D/M89D produced spaced patches that co-localized with ER markers (Kaiser et al., 2005). The VAPB-P56S mutation may exhibit similar loss of cellular processes and deterioration of ER morphology in ALS8. VAPB-P56S may block VAPBs binding to FFAT containing lipid binding or transfer proteins leading to loss of function and ER deterioration. An objective of the current study is to resolve if VAPB-P56S-induced deterioration of ER morphology inhibits vesicle trafficking of nucleoporins (Nups) and nuclear envelope (NE) proteins to their proper localization.

The VAP-FFAT interaction promotes synthesis of the ER membrane by regulating the lipid composition at the ER. A disruption of this process can lead to a change or collapse in ER morphology (Prosser et al., 2008). In 2005, a study addressing the severity of the FFAT-VAP binding on ER structure demonstrated that exogenous expression of FFAT-motifs from ORP3 and Nir2 causes formation of ER membrane stacks or whorls, while other proteins such as Nir3 rearranged ER structure (Amarilio et al., 2005). These results suggest that FFAT-containing proteins initiate dynamic changes in ER morphology. In ALS8, VAPB-P56S has been shown to produce insoluble cytoplasmic aggregates (Kanekura et al., 2006; Moumen et al., 2011)

Overexpression of VAPB-P56S in CHO cells has shown to form large ER aggregates (Prosser et al., 2008). Moreover, co-overexpression of VAPB-P56S with the FFAT motif from rat OSBP in CHO cells has been shown to resolve these large ER aggregates (Prosser et al., 2008). Although, it is not clear as to why these aggregates form, a study in 2007 demonstrated that mutant VAPB-P56S cannot interact with a green fluorescent protein (GFP)-tagged FFAT motif (Teuling et al., 2007). Although it is possible that the FFAT motif cannot interact with the VAPB protein because aggregation blocks FFAT from reaching VAPs binding site, it is clear that the VAP-FFAT interaction is crucial for ER morphology and regulating lipid synthesis at the ER (Teuling et al., 2007; Prosser et al., 2008; Amarilio et al., 2005).

The ER is Continuous with the NE

The outer nuclear membrane (ONM) is continuous with the rough-ER (Fig. 4A). Since mutant VAPB induces ER morphology defects and affects ER trafficking, the continuity between the ER and NE raises the possibility that transport of NE proteins might also be affected and contribute to the ALS8 disease pathogenesis. The NE divides eukaryotic cells into a nuclear and cytoplasmic compartment providing a selective permeable barrier between the compartments (Starvu et al., 2006). The nuclear envelope (NE) is comprised of two lipid bilayers. The inner nuclear membrane (INM) is attached to lamins, a family of structural support proteins in the nuclear arena and the ONM is continuous with the rough ER (Starvu et al., 2006). The INM and ONM are separated by a perinuclear space approximately 30nm wide that is continuous with the lumen of the ER (Starvu et al., 2006) (Fig. 4A). Local fusion between both membranes creates the aqueous nuclear pore complexes (NPCs) spanning both membranes for nucleocytoplasmic transport (Starvu et al., 2006). NPCs are around 125 MDa in size formed by approximately 30 Nups (Antonin et al., 2005). The NPC has an eight-fold rotational symmetry with three concentric rings: The cytoplasmic ring, the central ring and the nuclear ring. The nuclear and central rings

compose the nuclear basket (Fig. 4B). Shuttling between the cytoplasm and nucleus is a tightly regulated process with more than one million molecules passing through approximately 2-3 thousand nuclear pores per minute (Antonin et al., 2005). This process requires the interaction between Nups and nuclear localization signals in order to facilitate translocation. All proteins that are imported into the nucleus bear a nuclear localization signal (NLS) and all proteins that exported require a nuclear export sequence (NES) (Antonin et al., 2005).

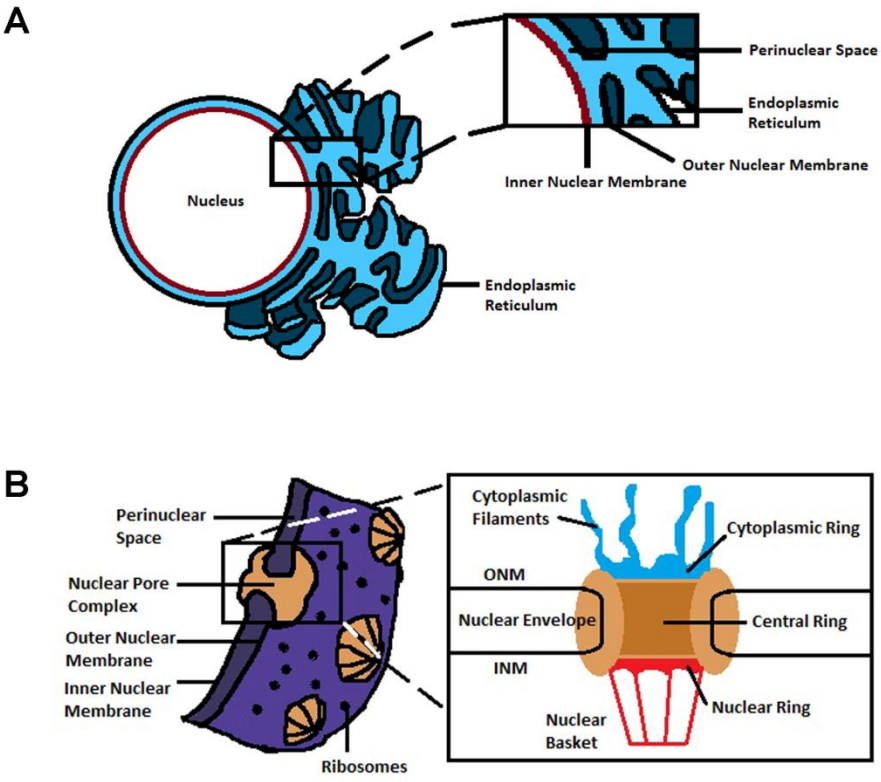

Figure 4. The ER is Continuous with the NE and the NPC Structure. (A) The outer nuclear membrane is continuous with the rough-ER and the perinuclear space is continuous with the lumen of the ER. (B) A diagram of the NPC structure.

Nucleoporins and Inner Nuclear Membrane Proteins

Each Nup of the NPCs holds specific functions. Pom121 is an integral membrane protein localized to the central ring of the NPC (Antonin et al., 2005). Pom121 functions in anchoring the NPC to the NE (Antonin et al., 2005). Gp210 is located at the central ring of the NPC (Antonin et al., 2005). Gp210 also anchors the NPC to the NE. To date, Gp210, Pom121 and Ndc1 are the three integral membrane proteins of the NPC anchoring the NPC to the NE (Antonin et al., 2005). Nup214 is localized at the cytoplasmic ring of the NPC (Xu et al., 2009). Lamin-B1 is part of a family of intermediate filaments which stabilize the NE and anchors nuclear membrane proteins to the scaffold of the INM (Holaska et al., 2006). Emerin is an integral protein of the INM expressed in almost all human cells belonging to the 'LEM domain' (LAP2/Emerin/MAN1) family of nuclear proteins (Holaska et al., 2006). Emerin binds to and co-localizes with A and B-type lamins in the INM which anchor Emerin for architectural, gene regulator and nuclear assembly roles (Holaska et al., 2006).

The NE is disassembled during open mitosis, and nuclear pores are equally divided to the two newly formed nuclei. Heightened NPC assembly occurs shortly thereafter to double the number of pores in the daughter cells. The rate of de novo synthesis progressively decreases during interphase. In post-mitotic cells, such as neurons, this mitotic renewal process is not followed. Research has not yet fully established what occurs to NPCs in post-mitotic cells; however, it has been shown that NPCs do not turn over appreciably in differentiated cells (D'Angelo et al., 2009). Some NPC proteins, however, can be exchanged at the NPC, others are extremely long lived and some are incorporated in the NPC the entire lifespan of a cell (D'Angelo et al., 2009). The current thesis focuses on interphase cells and the described NPC and NE proteins will be examined to illustrate the effects of VAPB-P56S on NPC and NE proteins.

Amyotrophic Lateral Sclerosis Disrupts the Nucleus

D'Angelo in 2009 showed that nuclear leakiness is accelerated during aging (D'Angelo et al., 2009). The effect of oxidative damage and age-related deterioration on the NPC was examined. Utilizing the environmental toxin paraquat induced oxidative damage by increasing the amount of reactive oxygen species (ROS) in *Caenorhabditis elegans* for six days (D'Angelo et al., 2009). The worms treated with paraquat exhibited a higher percentage and earlier onset of leaky nuclei by nuclear entry of the 70 kDa dextran when compared to controls not treated with paraquat. Also, older worms had increased nuclear permeability compared to young worms and addition of paraquat treatment increased nuclear leakiness (D'Angelo et al., 2009). Thus, age-related deterioration of NPCs leads to loss of the NPC selective permeability barrier (D'Angelo et al., 2009). This consequently results in the leak of cytoplasmic proteins into the nucleus. ALS is an adult-late onset disease; therefore, VAPB-P56S may increase nuclear permeability resulting from damage to NPCs and loss of nuclear integrity (D'Angelo et al., 2009).

In 2009, a study examined Nup distribution in anterior horn cells of patients with ALS (Kinoshita et al., 2009). The Nups examined were nup88, nup62, and nup153 (Kinoshita et al., 2009). They examined Nup distribution by antibody staining of the spinal cord of SALS and FALS patients. In control individuals, the Nups formed entirely smooth nuclear contours (Kinoshita et al., 2009). However, in cells of both SALS and FALS patients the nucleus was irregular and twisted with irregular nuclear contours (Kinoshita et al., 2009).

Ngsee's group in 2012 linked ALS8 to a dysfunction in NE structure (Tran et al., 2012). The NE of CHO fibroblasts overexpressing VAPB-P56S in the absence or present of the FFAT motif was analyzed by transmission electron microscopy (EM). In the absence of FFAT, CHO cells contained large empty vacuoles resembling expanded ER not observed in FFAT transfected cells. The NE

displayed a significant separation in distance between the ONM and INM in approximately 75% of non-FFAT transfected cells compared to control or FFAT transfected cells (Fig. 5) (Tran et al., 2012). The distance between the INM and ONM in VAPB-P56S transfected cells were as grand as 500 nm with an average of 160 ± 32 nm whereas VAPB-WT mean distance between the ONM and INM was 70 ± 5 nm (Tran et al., 2012). The results illustrated a defect in NE structure and are the foundation of the current thesis. A current objective is to examine VAPBs role in the transport of NPC and NE proteins. If VAPB plays a role, then VAPB-P56S may induce the separation of the ONM and INM by inhibiting the proper assembly of the NPC and transport of NE proteins which may contribute to the pathogenesis of ALS.

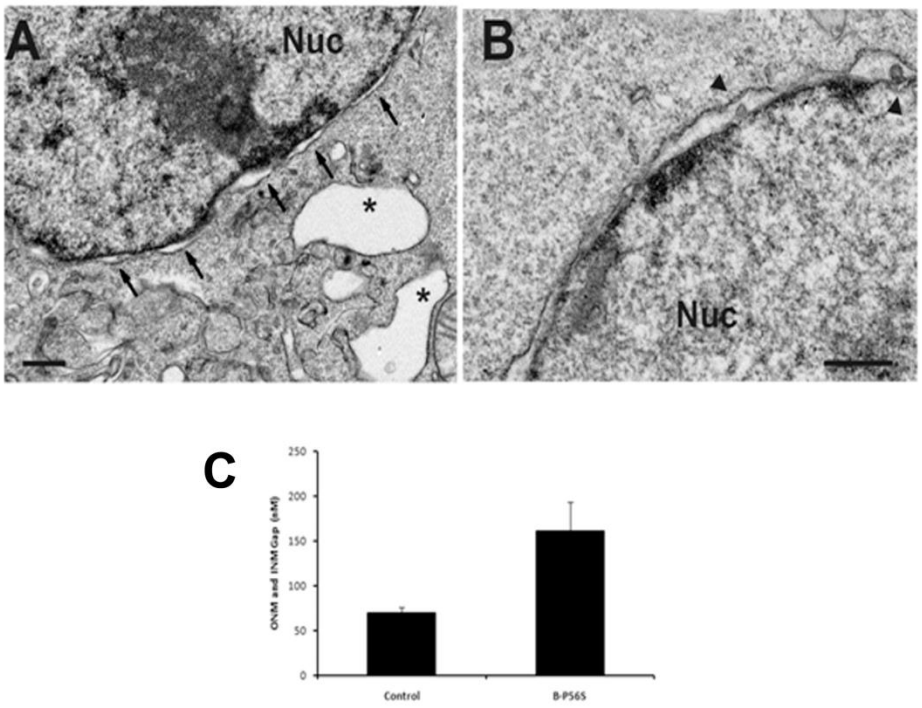

Figure 5. Over-expression of VAPB-P56S induces a NE defect. (A) Large vacuole-like membrane structures (*) and swelling of nuclear envelope (arrows) in mutant VAPB-P56S transfected CHO cells. (B) Magnified image of NE defect illustrating separation of the ONM and INM. (D) Quantification of distance between ONM and INM in control and mutant VAPB-P56S transfected cells. Values are given as the distance in nm ± S.E.M. (Tran et al., 2012).

Hypothesis and Objective

The main objective of this study is to identify and characterize the relationship between VAPB and the trafficking of NPC and NE proteins. Since VAPB-P56S causes a NE defect characterize by separation of the ONM and INM, I hypothesize that this could be caused by deterioration in NPC assemble. Some Nups and NE proteins are synthesized at the ER and then transit to the NE, I hypothesize that VAPB regulates this process. VAPB-P56S may disrupt Nup and NE protein transport from the ER resulting in loss of proper Nup and NE protein localization thus inducing a separation between the NEs INM and ONM. This may cause a defect in nucleocytoplasmic shuttling. Since binding to FFAT-motif containing lipid binding proteins is crucial for VAPB function, co-expressing the FFAT motif may counteract the mutations adverse effects.

In order to test this hypothesis, *in vitro* experiments were performed to examine the effects of VAPB-P56S on Nup and NE protein trafficking. The major method employed to address this issue involved transfecting VAPB-P56S DNA and subsequently analysing the cells morphology and protein localization by confocal microscope. The effect of P56S on Nup transport was examined using the Nups Gp210, Nup214, Pom121 and the INM proteins Emerin and Lamin-b1. Further, to address the function of VAPB on NPC and NE protein transport, we knocked down synthesis of VAPB using shRNA. If it is shown that Nups and NE proteins are retained in cytoplasmic VAPB-P56S-induced aggregates and are shown to be retained in the cytoplasm upon knockdown of VAPB, then the compartment in which NE and NPC proteins are retained must be characterized. Bu utilizing ERGIC-53-GFP, a marker for the ERGIC which displays both anterograde and retrograde transport, we can determine if the NPC and NE proteins are retained in this compartment. Thus, this will demonstrate if VAPB is implicated in the transport of proteins from the ERGIC. If the previous experiments indicate that NPC and NE proteins are in fact retained in the cytoplasm resulting in an altered NPC composition, the consequences of a defective NE and

NPC can be examined by utilizing the ligand-activated glucocorticoid receptor (GR). This will indicate if a defect in nucleocytoplasmic shuttling results due to VAPB-P56S or due to loss of VAPB function by knockdown of endogenous VAPB. A further objective of this study is to examine the biophysical properties of VAPB-P56S. It has been shown that the VAPB mutation induces a biophysical change resulting in insolubility of the protein. Upon co-transfection of the FFAT-motif, the adverse effects of VAPB-P56S are resolved. Therefore, I hypothesize that the co-overexpression of the FFAT-motif with VAPB-P56S may induce a change in VAPB-P56S biophysical properties manifested by proper VAPB function. Chinese hamster ovary (CHO) fibroblasts and HeLa cells were used throughout this study.

MATERIALS AND METHODS

DNA PLASMID CONSTRUCTS

Human VAPB cDNA

Human VAPB complimentary DNA (cDNA) coding for human VAPB-wild type and the P56S mutation of VAPB was previously produced by Dr. Derek C. Prosser (Prosser et al., 2008).

shRNA: pLKO.1 and shVAPB

Lentiviral pLKO.1 based plasmids were from Open Biosystems (Hunstville, AL, USA). TRCN0000152888 matched both human and mouse VAPB sequences. Empty pLKO.1 vector was used as a control. In some cases, the shRNA plasmids were co-transfected with monomeric RFP (mRFP) to identify the transfected cells.

The FFAT Motif and the AAAT motif

The FFAT motif of rabbit OSBP (residue 347-468) and the AAAT motif of rabbit OSBP was produced by Dr. Derek C. Prosser (Prosser et al., 2008).

Emerin-GFP

The Emerin cDNA was obtained from Open Biosystems (Hunstville, AL, USA) and then subsequently cloned into pEGFP-C1 at the *BspE1* and *BamH1* sites by Duvinh Tran.

Nucleoporins and INM Protein Plasmids

The Gp210-GFP DNA plasmid was purchased as prGp210(s)-EGFP3-(TM+CT) with the triple GFP tag on the C-terminus of Gp210. Nup214-GFP DNA plasmid was obtained as pNup214-EGFP with the GFP tag on the C-terminus of Nup214. Subsequently, the Nup214-GFP DNA plasmid was cloned into an mRFP-N1 plasmid at the *EcoR1* and *Age1* sites. Pom121-GFP DNA plasmid was obtained as pPom121-EGFP3 with the GFP tag on the C-terminus of Pom121. Lamin-B1-GFP DNA

plasmid was obtained as pEGFP-LaminB1 with the GFP tag on the N-terminus of Lamin-B1. All these plasmids were obtained from EUROSCARF (Frankfurt, Germany).

ERGIC-53-GFP

The ERGIC-53-GFP DNA plasmid was obtained from the lab of Dr. Hans-Peter Hauri.

GR-GFP

The Glucocorticoid Receptor (GR) tagged to GFP was obtained from the lab of Dr. Robert J.G. Hache from the University of Ottawa, Ottawa Health Research Institute

PRIMARY ANTIBODIES

ERGIC-53 primary antibody was obtained from SIGMA-Aldrich (St. Louis, MO, USA) as Anti-ERGIC-53/p58 polyclonal antibody produced in rabbit and was utilized at a dilution of 1:50. Golgin-97 primary antibody was obtained from ABCAM as rabbit polyclonal antibody to Golgin 97 and was diluted at 1:50. Mab414 primary antibody was obtained from ABCAM (Covance, Princeton, NJ, USA) as mouse monoclonal antibody to Nuclear Pore Complex Proteins and was diluted at 1:100. Emerin primary antibody was obtained from Developmental Studies Hybridoma Bank (Iowa City, IA, USA) as MANEM1 and was diluted at 1:50. VAPB, either WT or mutant P56S, constructs were Flag-epitope tagged and were visualized with mouse anti-FLAG primary antibody (Applied Biological Materials, Richmond, BC, Canada) diluted at 1:1000.

SECONDARY ANTIBODIES

Goat anti-mouse or goat anti-rabbit 488(green) or 594 (red) was obtained from Invitrogen (Carlsbad, CA, USA) and diluted at 1:250.

CELL CULTURE

CHO and Hela

Chinese Hamster Ovary (CHO-K1) fibroblasts were maintained in minimum essential medium (MEM) α (Invitrogen) and HeLa cells were maintained in Dulbecco's modified Eagle's medium (DMEM) (Invitrogen). Both cell lines were supplemented with 5% fetal bovine serum (FBS) (Invitrogen), 100 U/ml penicillin and 100µg/ml streptomycin (Invitrogen) and maintained at 37°C with 5% CO_2.

DNA TRANSFECTION

CHO fibroblasts were seeded at $0.8x10^5$ cells per well on 12mm glass coverslips (Fisher) in a 24-well plate 16 hours prior to transfection. CHO fibroblasts were transfected with 500 ng of DNA plasmid and 1 µl LipofectAMINE reagent (Invitrogen) in 200 µl Opti-MEM (Invitrogen) for 4 hours. After 4 hours, the transfection mix was removed and replaced with complete MEM α described earlier. Similarly, HeLa cells were seeded and transfected equivalently; however, after 4 hours the transfection mix was removed and replaced with complete DMEM medium.

IMMUNOCYTOCHEMISTRY

Forty-eight hours after the cells were transfeced, the cells were washed with (1X) 0.0067 M phosphate-buffered saline (PBS) (Fisher). To fix the cells, 4% paraformaldehyde from Cedarlane in PBS was placed on the cells for 30 minutes. Following, the cells were washed 3 times each time for 3 minute with PBS wash solution (PBS containing 0.1 M glycine (Roche) and 0.01 % sodium azide/NaN_3 (JT Baker)). The cells were then permeabilized (PBS containing 0.4% saponin (Sigma), 1% bovine serum albumin (Sigma), 2% normal goat serum (Invitrogen) and 0.01% sodium azide/NaN_3 (JT Baker)) for 30 minutes followed by 3 washes for 3 minutes with PBS wash. The cells were then incubated with the appropriate primary antibody required for the

experiment for 1 hour at room temperature or overnight at 4°C. Subsequently, the cells were washed with PBS wash solution 3 times, 3 minutes each time and then incubated with the appropriate secondary antibody required for the experiment for 1 hour followed by washing with PBS wash solution 3 times. Further, the cells were equilibrated using equilibration buffer (1X PBS, 30% glycerol and 0.01% NaN_3) for 10 minutes. Lastly, the coverslips were mounted in SlowFade Gold reagent or SlowFade Gold reagent with DAPI depending on the experiment (Invitrogen) on 3x1x1 mm glass microscope slides (Fisher) and fixed with nail polish.

IMAGE COLLECTION

Images were captured using a Zeiss LSM510 META laser scanning confocal microscope equipped with a 60x oil-immersion objective and LSM510 image acquisition software.

EXPERIMENTS

(A) Characterizing the Functional Role of VAPB in Transport of INM and NPC Proteins

Gp-210, Nup-214 and Emerin are Mis-localized in VAPB-P56S Transfected Cells

DNA Transfection

To determine if VAPB is required for transport of INM and NPC proteins and VAPB-P56Ss effect on INM and NPC localization, CHO and HeLa were co-transfected with Flag-epitope tagged VAPB-WT or VAPB-P56S and with Emerin-GFP or Gp210-GFP or Nup214-GFP or Lamin-B1-GFP.

Immunocytochemistry

The cells were incubated with mouse anti-FLAG (1:1000) (Applied Biological Materials) for VAPB primary antibody and the protein was visualized with goat anti-mouse Alexa Fluor 594-(1:250) secondary antibody (Invitrogen). Emerin-GFP, Gp210-GFP, Nup214-GFP and Lamin-B1-GFP were visualized by their green-fluorescent protein tag (GFP).

The FFAT Motif Rescues Mis-localized NE and NPC Proteins of VAPB-P56S

DNA Transfection

It has been shown that simultaneous over-expression of the FFAT-motif with mutant VAPB resolves the abnormal ER morphology and restores ER-Golgi trafficking (Prosser et al., 2008). Thus, here I address if this could resolve the effects of VAPB-P56S on Nups and NE proteins. CHO and HeLa cells were co-transfected with Emerin-GFP or Gp210-GFP or Nup214-GFP and with either Flag-epitope tagged VAPB-WT or VAPB-P56S and with pcDNA3.1 (+)-Myc empty vector or pcDNA3.1 (+)-Myc/OSBP-FFAT for conditions that were in the absence or presence of FFAT, respectively.

Immunocytochemistry

The cells were incubated with mouse anti-FLAG (1:1000) (Applied Biological Materials) for VAPB primary antibody and the protein was visualized with goat anti-mouse Alexa Fluor 594-(1:250) secondary antibody (Invitrogen). Emerin-GFP, Gp210-GFP, Nup214-GFP and Lamin-B1-GFP were visualized by their green-fluorescent protein tag (GFP).

Emerin, Pom-121- and Nup-214 are mis-localized upon siVAPB knockdown

DNA Transfection

To determine whether transport defect is due to loss of VAPB function and to exclude non-specific sequestration of NE proteins with aggregated mutant VAPB, I examined the distribution of Nups and NE proteins upon siRNA knockdown of endogenous VAPB. If similar phenotypes are observed in the siRNA cells compared to the P56S cells then I can address if the P56S mutation causes a loss of function of the WT protein. CHO and HeLa cells were co-transfected with either Pom121-GFP or Nup214-GFP and with either empty lentiviral pLKO.1 vector control or with

siRNA. For the localization of Emerin, cells were co-transfected with either pLKO.1 or shRNA and with monomeric RFP (MRFP) to identify the transfected cells.

Immunocytochemistry

Pom121 + siVAPB and Nup214 + siVAPB

There was no primary or secondary antibody used because Pom121-GFP or Nup214-GFP was visualized by its green-fluorescent protein tag (GFP).

Emerin + siVAPB

Cells were incubated with mouse anti-Emerin (1:1000) primary antibody (Applied Biological Materials) for endogenous Emerin and the protein was visualized with goat anti-mouse Alexa Fluor 488-(1:250) secondary antibody (Invitrogen). Emerin was visualized by green fluorescents and mRFP was red.

(B) Characterizing the compartment in which INM and NPC proteins are retained

VAPB is Localized to the ERGIC

DNA Transfection

To determine whether VAPB co-localized with the ERGIC, CHO and HeLa cells were co-transfected with Flag-epitope tagged VAPB-WT and with ERGIC-53-GFP.

Immunocytochemistry

The cells were incubated with mouse anti-FLAG (1:1000) (Applied Biological Materials) for VAPB primary antibody and the protein was visualized with goat anti-mouse Alexa Fluor 594-(1:250) secondary antibody (Invitrogen). ERGIC-53 was visualized by its green-fluorescent protein tag (GFP).

Cell Phenotype Quantification and Statistical Analysis

Cells exhibiting punctate spots in the cytoplasm where quantified as ERGIC containing cells. Only low level of VAPB-WT expressing cells were examined to avoid over-expression artifacts and to examine if VAPB co-localizes with the ERGIC puncta. After images were capture, statistical analysis was examined utilizing ImageJ software's intensity correlation analysis which provides a Pearson's correlation coefficient that quantifies the correlation between two channels. The values for Pearson's will range from 1 to -1. A value of 1 represents perfect positive correlation, -1 represents perfect negative correlation and zero represents random localisation. Further, Mander's overlap coefficient was also calculated to quantify for co-localisation. This method generates a figure between zero and 1, with 1 representing a high co-localisation between two channels. These two methods of quantification were utilized to find co-localisation between VAPB-WT and ERGIC-53. In order to precisely quantify a correlation between the VAPB signal and the ERGIC-53 signal, the Golgi was excluded by examining, through ImageJ software, a Region of Interest (ROI). This was performed because the Golgi was seen to be devoid of VAPB and my interest is on examining VAPB containing compartments such as the ERGIC. This method was carried on for every subsequent experiment involving a correlation analysis with the ERGIC.

VAPB-P56S and siVAPB Compromises the ERGIC

DNA Transfection

To determine the effects of VAPB-P56S on the ERGIC HeLa cells were co-transfected with either Flag-epitope tagged VAPB-WT or VAPB-P56S and with ERGIC-53-GFP. For the siVAPB condition, HeLa cells were co-transfected with ERGIC-53-GFP and empty pLKO.1 or siVAPB.

Immunocytochemistry

VAPB-P56S and ERGIC-53-GFP

The cells were incubated with mouse anti-FLAG (1:1000) (Applied Biological Materials) for VAPB primary antibody and the protein was visualized with goat anti-mouse Alexa Fluor 594-(1:250) secondary antibody (Invitrogen). ERGIC-53 was visualized by its green-fluorescent protein tag (GFP).

siVAPB and ERGIC-53-GFP

No primary or secondary antibodies were utilized. ERGIC-53 was visualized by its green-fluorescent protein tag (GFP).

Cell Phenotype Quantification and Statistical Analysis

Mutant VAPB-P56S expressing cells were examined to identify any change in correlation between VAPB and the ERGIC. Firstly, after images were capture, statistical analysis was performed to calculate the Pearson's correlation coefficient and Mander's overlap coefficient for co-localisation as previously described. These two methods of quantification were utilized to find co-localisation between VAPB-P56S and ERGIC-53.

Secondly, VAPB-P56S and siVAPB knockdown cells exhibited expanded punctate inclusions throughout the cytoplasm. The siVAPB induced expansion and disruption of the ERGIC was quantified by counting 200 cells for each condition. Values obtained represent the percentage of HeLa cells containing ERGIC expanded aggregates ± S.E.M., n=3. Statistical analysis comparing pLKO.1 to shVAPB expressing cells was performed using a Student t-test and a p-value <0.05 was considered significant.

Lastly, the expanded ERGIC inclusions evident in HeLa cells were measured by their Feret's diameter in nm for pLKO.1 control cells and for shVAPB cells and for VAPB-WT and VAPB-P56S

overexpressing cells. Values are represented as the frequency of HeLa cells containing ERGIC of a given diameter in nm ± S.E.M., n=3. Statistical analysis comparing pLKO.1 to shVAPB and empty to VAPB-WT and VAPB-P56S overexpressing cells was performed using a Student t-test and a p-value <0.05 was considered significant.

The ERGIC Distortion is not due to Over-Expression of ERGIC-53

DNA Transfection

In order to eliminate the possibility that the expansion seen in the ERGIC may be due to over-expression, I repeated the previous experiments with an antibody towards the ERGIC. For the VAPB condition, HeLa cells were transfected with either Flag-epitope tagged VAPB-WT or VAPB-P56S. For the siVAPB condition, HeLa cells were co-transfected with ERGIC-53-GFP and empty pLKO.1 or siVAPB.

Immunocytochemistry

VAPB and ERGIC-53 Antibody

The cells were incubated with mouse anti-FLAG (1:1000) (Applied Biological Materials) for VAPB and with anti-ERGIC-53/p58 a polyclonal antibody produced in rabbit primary antibodies. Subsequently, the VAPB protein was visualized with goat anti-mouse Alexa Fluor 594(red)-(1:250) secondary antibody (Invitrogen) and the ERGIC was visualized with goat anti-rabbit Alexa Fluor 488 (green)-(1:250) secondary antibody (Invitrogen).

siVAPB and ERGIC-53 Antibody

The cells were incubated with anti-ERGIC-53/p58 primary antibody and the ERGIC was visualized with goat anti-rabbit Alexa Fluor 488 (green)-(1:250) secondary antibody (Invitrogen). The coverslips were mounted in SlowFade Gold reagent with DAPI (Invitrogen).

Cell Phenotype Quantification and Statistical Analysis

After images were capture, statistical analysis performed calculated the Pearson's correlation coefficient and Mander's overlap coefficient to quantify for co-localisation as described previously. These two methods of quantification were utilized to find co-localisation between VAPB-WT and ERGIC-53 and between VAPB-P56S and ERGIC-53.

Further, the expanded ERGIC inclusions evident in HeLa cells were measured by their Feret's diameter in nm as described previously.

Emerin, Mab414, and Nup214-RFP Co-localize with the ERGIC

DNA Transfection

To address if Nups and NE proteins are transported to the ERGIC, Hela cells were co-transfected with pLKO.1 empty vector and ERGIC-53-GFP to examine Emerin and Mab414 distribution. Subsequently, HeLa cells were co-transfected with pLKO.1, ERGIC-53-GFP, and Nup214-RFP to examine Nup214 distribution.

Immunocytochemistry

Emerin + ERGIC-53-GFP

The cells were incubated with mouse anti-Emerin(MANEM1) (1:50) (Developmental Studies Hybridoma Bank) primary antibody towards endogenous Emerin and the Emerin protein was visualized with goat anti-mouse Alexa Fluor 594(red)-(1:250) secondary antibody (Invitrogen). The coverslips were mounted in SlowFade Gold reagent with DAPI (Invitrogen). The ERGIC was visualized by its GFP tag(green).

Mab414 + ERGIC-53-GFP

The cells were incubated with mouse anti-Mab414 (1:50), a monoclonal antibody that recognizes several FG repeat Nup, primary antibody and Mab414 was visualized with goat anti-

mouse Alexa Fluor 594(red)-(1:250) secondary antibody (Invitrogen). The coverslips were mounted in SlowFade Gold reagent with DAPI (Invitrogen). The ERGIC was visualized by its GFP tag(green).

Nup214-RFP + ERGIC-53-GFP

No primary or secondary antibody was required and the ERGIC was visualized by its GFP tag (green) and Nup214 was visualized by its RFP tag (red).

Cell Phenotype Quantification and Statistical Analysis

After images were capture, statistical analysis performed calculated the Pearson's correlation coefficient and Mander's overlap coefficient to quantify for co-localisation as described previously. These two methods of quantification were utilized to find co-localisation between Emerin and ERGIC-53, Mab414 and ERGIC-53 and Nup214 and ERGIC-53.
Further, the size of the ERGIC-53-GFP, Mab414 and Emerin punctate inclusions in the cytoplasm of HeLa cells were measured by their Feret's diameter (nm) as described previously.

Emerin, Mab414, and Nup214 are Retained at the ERGIC upon shVAPB

DNA Transfection

To verify that Nups are retained at the ERGIC in a VAPB-dependent manner. Hela cells were co-transfected with shVAPB and ERGIC-53-GFP and stained for endogenous Emerin or Mab414 to examine Emerin and Mab414 distribution. Subsequently, HeLa cells were co-transfected with shVAPB, ERGIC-53-GFP, and Nup214-RFP to examine Nup214 distribution.

Immunocytochemistry

Emerin + ERGIC-53-GFP + shVAPB

The cells were incubated with mouse anti-Emerin(MANEM1) (1:50) (Developmental Studies Hybridoma Bank) primary antibody towards endogenous Emerin and Emerin was visualized with goat anti-mouse Alexa Fluor 594(red)-(1:250) secondary antibody (Invitrogen). The coverslips were mounted in SlowFade Gold reagent with DAPI (Invitrogen). The ERGIC was visualized by its GFP tag (green).

Mab414 + ERGIC-53-GFP + shVAPB

The cells were incubated with mouse anti-Mab414 (1:50) primary antibody and Mab414 was visualized with goat anti-mouse Alexa Fluor 594(red)-(1:250) secondary antibody (Invitrogen). The coverslips were mounted in SlowFade Gold reagent with DAPI (Invitrogen). The ERGIC was visualized by its GFP tag (green).

Nup214-RFP + ERGIC-53-GFP + shVAPB

The application of a primary and secondary antibody was not required. The coverslips were mounted in SlowFade Gold reagent with DAPI (Invitrogen). The ERGIC was visualized by its GFP tag (green) and Nup214 was visualized by its RFP tag (red).

Cell Phenotype Quantification and Statistical Analysis

After images were capture, statistical analysis performed calculated the Pearson's correlation and Mander's overlap coefficients to quantify for co-localisation as described previously. These two methods of quantification were utilized to find co-localisation between Emerin and ERGIC-53, Mab414 and ERGIC-53 and Nup214 and ERGIC-53 in all VAPB knockdown conditions.

Further, siVAPB knockdown cells exhibited expanded punctate inclusions of ERGIC-53-GFP, Mab414 and Emerin. The expanded ERGIC inclusions were measured by their Feret's diameter (nm) as described previously.

ERGIC-53 Accumulates at the ERGIC at 15°C and Retains Emerin

DNA Transfection

HeLa cells were transfected with ERGIC-53-GFP.

15°C Temperature Trapping Conditions and Immunocytochemistry

Incubation at 15°C is known to reversible accumulate ERGIC-53 at the ERGIC by blocking retrograde transport to the ER (Hauri et al., 2000; Ben-Tekaya et al 2005). To address if NE proteins are transported via vesicular transport to the ERGIC and then to the NE, forty-eight hours after transfection HeLa cells were transferred from 37°C to 15°C from 0 to 8 hours. At each hour, starting at zero hours as the control, the cells were fixed and stained with mouse anti-Emerin(MANEM1) (1:50) (Developmental Studies Hybridoma Bank) primary antibody towards endogenous Emerin and with goat anti-mouse Alexa Fluor 594(red)-(1:250) secondary antibody (Invitrogen). The coverslips were mounted in SlowFade Gold reagent with DAPI (Invitrogen). The ERGIC was visualized by its GFP tag (green).

Cell Phenotype Quantification

In control cells, ERGIC-53 greatly co-localized at the Golgi and with punctate staining throughout the cytoplasm. Emerin formed a ring-like pattern along the rim of the NE in control cells. For quantification purposes, cells exhibiting an expanded ERGIC and cells displaying the loss of the characteristic Emerin ring along the rim of the NE upon the 15°C shift were chosen as distorted cells.

(C) Consequence of a Defective NE and NPC Assembly

VAPB-P56S causes a delay in nuclear translocation of activated GR and the FFAT motif rescues the delay

DNA Transfection

To monitor the effects of VAPB on nucleocytoplasmic shuttling, CHO fibroblasts were co-transfected with GR-GFP and with either pFlag-CMV2 vector for the control or Flag-epitope tagged VAPB-WT or VAPB-P56S. In addition, the cells were co-transfected with pcDNA3.1 (+)-Myc empty vector or pcDNA3.1 (+)-Myc/OSBP-FFAT for conditions that were in the absence or presence of FFAT, respectively.

Dexamethasone Administration and Immunocytochemistry

Immediately after transfection, the cells were washed with (1X) 0.0061 M phosphate-buffered saline (PBS) (Fisher). Following, the cells were maintained at 37°C in minimal essential medium α, and supplemented with 100 U/ml penicillin, 100μg/ml streptomycin and 5% charcoal stripped FBS. Charcoal stripped FBS was used to eliminate any extra glucocorticoids that might activate GR prematurely. Forty-eight hours after transfection, the cells were washed 5 times with (1X) PBS (Fisher) then incubated in serum-free medium for 2 hours. Subsequently, 1μm of Dex was added and cells were fixed every 15 minutes from time 0 to 1 hour. Cells were stained with mouse anti-FLAG (1:1000) (Applied Biological Materials) for VAPB primary antibody and with goat anti-mouse Alexa Fluor 594-(1:250) secondary antibody (Invitrogen). The coverslips were mounted in SlowFade Gold reagent with DAPI (Invitrogen). GR-GFP was visualized by its green-fluorescent protein tag (GFP).

Quantification of GR Localization

Using ImageJ software, the percentage of GFP fluorescence in the nucleus was taken by the integrated density of the GFP signal localized to the nucleus outlined by DAPI staining relative to the total integrated density of the GFP signal of the whole cell. An average of 86 cells was quantified for each condition and values are represented as percentage of CHO cells containing 61-100% of the GR-GFP signal in the nucleus at each specific time point ± S.EM. n=3. Statistical analysis comparing FLAG or VAPB-WT to VAPB-P56S expressing cells were performed using a Student t-test and a p-value <0.05 was considered significant. An average of 68 cells was quantified for each condition in the presence of FFAT, and the same statistical analysis was performed.

VAPB Knockdown with siVAPB Demonstrates a Delay in GR Nuclear Entry

DNA Transfection

To monitor the effects of knocking down endogenous VAPB on nucleocytoplasmic shuttling, HeLa cells were co-transfected with GR-GFP and with pLKO.1 empty control or siVAPB.

Dexamethasone Administration and Immunocytochemistry

Immediately after transfection, the cells were maintained as described in the previous GR-GFP experiment. Forty-eight hours after transfection, Dex administration and the fixing and mounting of cells was applied as described in the previous GR-GFP experiment. However, the application of a primary or secondary antibody was not required.

Quantification of GR Localization

The method employed to quantify GR localization in the previous GR-GFP experiment was followed here. However, an average of 65 cells was quantified for each condition. Statistical

analysis comparing pLKO.1 and GR-GFP to shVAPB and GR-GFP expressing cells was performed using a Student t-test and a p-value <0.05 was considered significant.

VAPB Knockdown with shVAPB Increases GR Nuclear Translocation Time

DNA Transfection

To monitor the effects of knocking down endogenous VAPB on nucleocytoplasmic shuttling, a live-imaging technique to visualize the translocation of activated GR was performed. HeLa cells were seeded at $2.4x10^5$ cells on 35 mm petri dishes with 14mm microwell glass bottom culture dishes (MatTek) 16 hours prior to transfection. HeLa cells were transfected with 1500 ng of DNA plasmid and 3 µl LipofectAMINE reagent (Invitrogen) in 600 µl Opti-MEM (Invitrogen) for 4 hours. The cells were co-transfected with GR-GFP and with pLKO.1 empty control or siVAPB.

Dexamethasone Administration and Live Imaging Technique

Immediately after transfection, the cells were washed then maintained as in the previous GR experiment. Forty-eight hours after transfection, Dex was administered as in the previous GR experiment. However, the cells were immediately imaged live from time 0 to 1 hour with an image captured every 60 seconds. GR-GFP positive cells were defined as transfected cells and were visualized by GRs green-fluorescent protein tag (GFP).

Quantification of GR Localization

Using ImageJ software, the percentage of GFP fluorescence in the nucleus was taken by the integrated density of the GFP signal localized to the nucleus outlined by DAPI staining relative to the total integrated density of the GFP signal of the whole cell for each minute. The GFP intensity of six cells were quantified for each condition and values are represented as percentage of GR-GFP signal in the nucleus at each specific time point ± S.EM., n=6 for each

condition. Statistical analysis comparing pLKO.1 and GR-GFP to shVAPB and GR-GFP expressing cells was performed using a Student t-test and a p-value <0.05 was considered significant.

(D) Addressing the biophysical properties of the P56S mutation in VAPB

FFAT Changes the Solubility Properties of VAPB-P56S

DNA Transfection

To address why overexpressing the FFAT motif resolves VAPB-P56S induced ER aggregates and inhibition on vesicular transport between the ER and the Golgi, the biophysical properties of VAPB-P56S was examined. HeLa cells were seeded at $1.3x10^6$ cells in 10 cm tissue culture dishes (Sarstedt) 16 hours prior to transfection. Cells were co-transfected with Flag-epitope tagged VAPB-WT or Flag-epitope tagged VAPB-WT plus pcDNA3.1 (+)-Myc/OSBP-FFAT or Flag-epitope tagged VAPB-P56S or Flag-epitope tagged VAPB-P56S plus pcDNA3.1 (+)-Myc/OSBP-FFAT.

Collection of Cell Lysate

Forty-eight hours after transfection, cells were washed in PBS, scraped and centrifuged at 1,500x g for 5 min at 4°C. Cell pellet was re-suspended in 50 mM Tris-HCl pH7.5, 150 mM NaCl, 2mM EDTA, and 1% Triton X-100 and incubated on ice for 20min. Cells were centrifuged at 120,000x g for 30 min at 4°C. The collected supernatant held the Triton X-100-soluble fraction. The pellet was then re-suspended in 50 mM Tris-HCl ph 7.5, 150 mM NaCl, 2 mM EDTA, and 1% SDS and centrifuged at 120,000x g for 30 min at 4°C (Moumen et al., 2011). The supernatant collected was the SDS fraction. Basic western blot procedures were performed once both fractions were collected.

Immunoblotting

Protein concentration was determined using Bio-Rad DC Protein Assay (Bio Rad). Twenty Five µg of total protein for each condition was loaded onto SDS-PAGE vertical slab gels. The gels consisted of 12.5% acrylamide separating gel and 4% acrylamide stacking gel. Following SDS-PAGE, proteins were transferred to nitrocellulose membranes and the membrane was then blocked in blocking buffer (5% skim milk made with 1X Western Wash (150mM NaCl and 10mM Tris-HCl pH 7.5)) for 1 hour. Blots were then incubated overnight with mouse anti-FLAG (1:1000) (Applied Biological Materials) for VAPB primary antibodies diluted in blocking buffer. Subsequently, blots were incubated for 1 hour with Alexa-488-conjugated goat anti-mouse (1:2000) secondary antibodies diluted in blocking buffer. Following, blots were washed three times with 1X Western Wash and then imaged.

Image Collection

All blots were visualized with a Typhoon 8600 variable mode imager (Molecular Dynamics).

RESULTS

Characterizing the Functional Role of VAPB in Transport of INM and NPC Proteins

Gp210, Nup214, and Emerin are mis-localized in VAPB-P56S transfected cells

Since there was a NE defect in mutant VAPB over-expressing cells characterized by the separation of the ONM and the INM of the NE, I examined the distribution of Nups as a possible cause since the nuclear pores help maintain the close apposition by spanning the two nuclear membranes. The transport of NPC and INM proteins might be disrupted by mutant VAPB. I examined two Nups: Gp210 is an integral membrane protein anchoring the NPC with the nuclear membrane (Stavru et al., 2006) and Nup214 which forms the structural scaffold. To determine if trafficking of other NE proteins is also affected, I examined the distribution of Emerin, a structural integral membrane protein of the INM that shuttles between the ER and the INM (Zuleger et al., 2011). To confirm the localization of Nups and NE proteins, CHO and HeLa cells were co-transfected with Emerin-GFP, Gp210-GFP, Nup214-GFP or Lamin-B1-GFP and with either empty vector control, VAPB-WT or VAPB-P56S.

In empty vector and VAPB-WT overexpressing cells, Gp210-GFP formed a ring-like pattern encompassing the rim of the NE as well as localized to scattered cytoplasmic puncta (Fig. 6A). In contrast, Gp210-GFP was excluded from the NE and retained in mutant VAPB dilated membranes in the cytoplasm (Fig. 6A). Similarly, Nup214-GFP was localized to the NE in empty vector and VAPB-WT transfected cells, but sequestered in mutant VAPB containing aggregates (Fig 7A). Emerin-GFP formed a ring-like pattern along the rim of the NE in both control and VAPB-WT overexpressing cells (Fig 8A). In contrast, Emerin was retained in dilated cytoplasmic membranes and excluded from the NE in mutant VAPB overexpressing cells (Fig. 8A). This effect is not cell line specific as this was seen in CHO and HeLa cells. Thus, the transport of these two

Nups and Emerin is defective and they are retained in mutant VAPB-induced dilated membranes. Therefore, the transport of NPC and INM proteins is disrupted and this may be the cause of the separation between the INM and ONM. Lamin-B1 distribution was not altered by VAPB-WT or VAPB-P56S overexpression (Fig. 9). In VAPB-WT cells, Lamin-B1 formed a stable ring-like pattern around the NE which was not distorted by VAPB-P56S (Fig. 9).

The FFAT motif rescues mis-localized NE and NPC proteins of VAPB-P56S

It has previously been shown that simultaneous over-expression of the FFAT-motif with mutant VAPB resolves the abnormal ER morphology and restores ER-Golgi trafficking (Prosser et al., 2008). Thus, I hypothesize that this could also resolve the effects of the mutation on Nups and NE proteins. CHO and Hela cells were co-transfected with either Emerin-GFP, Gp210-GFP, or Nup214-GFP and with either empty vector control, VAPB-WT or VAPB-P56S in the presence of the FFAT motif from rabbit OSBP.

Normal nuclear localization of both Gp210-GFP and Nup214-GFP were restored upon co-overexpression of the FFAT fragment with VAPB-P56S (Fig. 6B and Fig 7B, respectively). Co-overexpression of FFAT also restored Emerin localization to the NE in mutant VAPB co-overexpressing cells (Fig. 8B). Thus, the FFAT motif can resolve the formation of VAPB-induced aggregates and relieve the transport defect of these two Nups and Emerin.

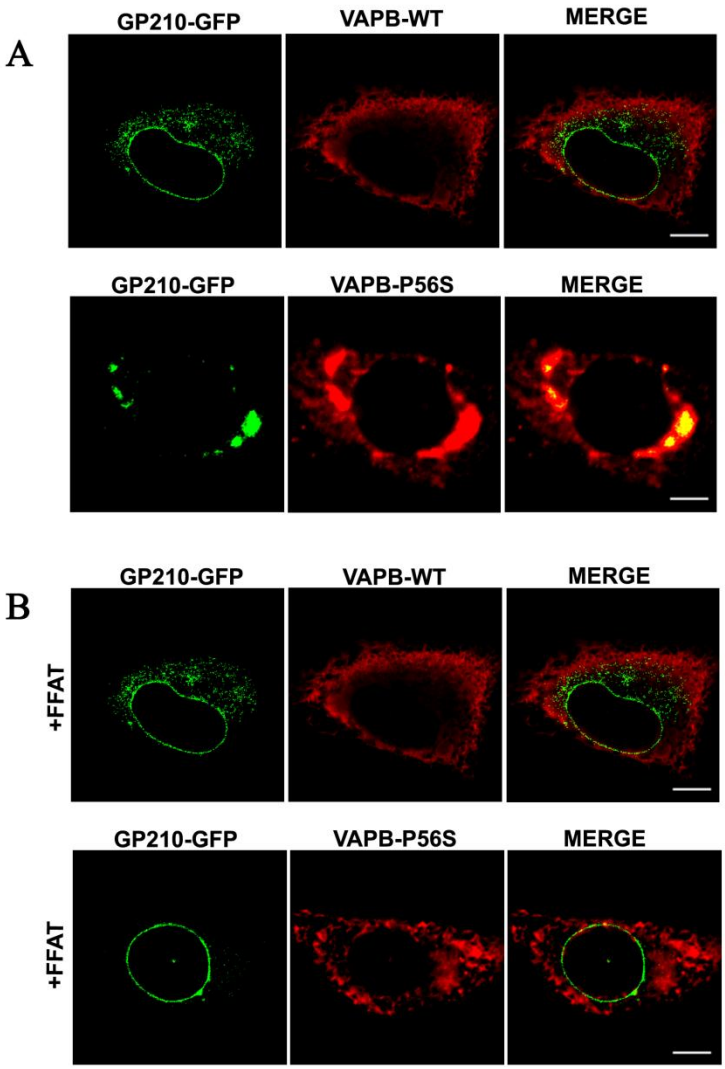

Figure 6. NE proteins are retained in mutant VAPB-containing membranes and restored by FFAT motif. (A) CHO cells were co-transfected with FLAG-tagged VAPB-WT or P56S and gp210-GFP. 48 hours after transfection the cells were fixed with 4% paraformaldehyde, stained with anti-FLAG (red) then mounted. Images were collected using a Zeiss LSM510 META laser scanning confocal microscope. (B) FFAT was co-transfected with FLAG-tagged VAPB -WT or P56S and gp210-GFP and cells were fixed, stained and imaged as in (A). Scale bar, 10μm.

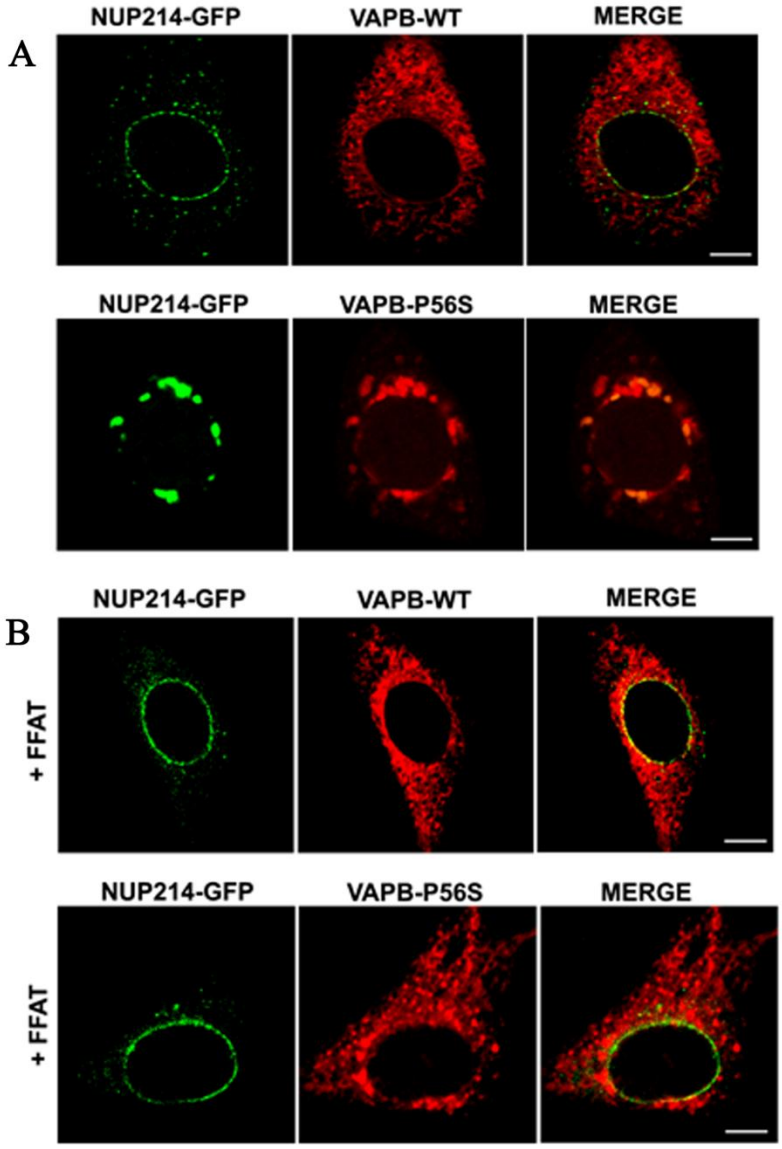

Figure 7. NE proteins are retained in mutant VAPB-containing membranes and restored by FFAT motif. (A) CHO cells were co-transfected with FLAG-tagged VAPB-WT or P56S and nup214-GFP. 48 hours after transfection the cells were fixed with 4% paraformaldehyde, stained with anti-FLAG (red) and moutned. Images were collected using a Zeiss LSM510 META laser scanning confocal microscope. (B) FFAT was co-transfected with FLAG-tagged VAPB -WT or P56S and nup214-GFP and cells were stained, fixed and imaged as in (A). Scale bar, 10μm.

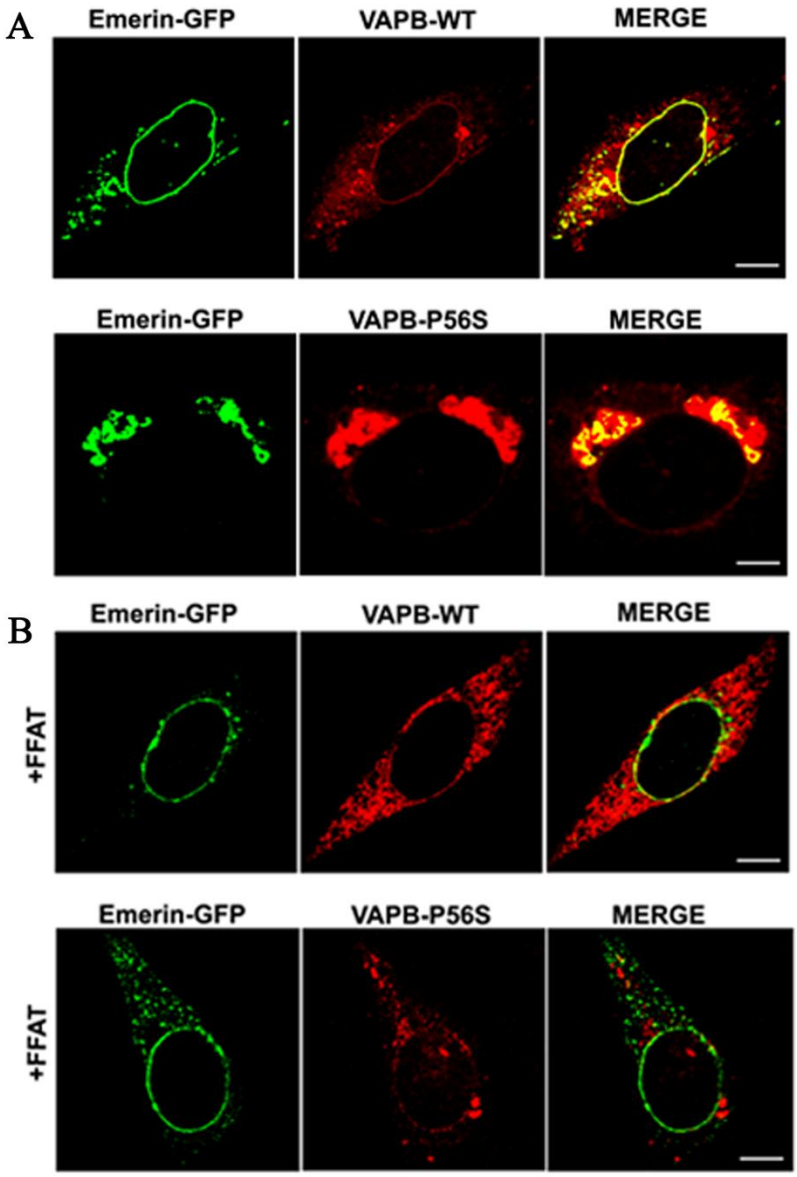

Figure 8. NE proteins are retained in mutant VAPB-containing membranes and restored by FFAT motif. (A) CHO cells were co-transfected with FLAG-tagged VAPB-WT or P56S and Emerin-GFP. 48 hours after transfection the cells were fixed with 4% paraformaldehyde then stained with anti-FLAG (red) and mounted. Images were collected using a Zeiss LSM510 META laser scanning confocal microscope. (B) FFAT was co-transfected with FLAG-tagged VAPB -WT or P56S and Emerin-GFP and cells were fixed and imaged as in (A). Scale bar, 10μm.

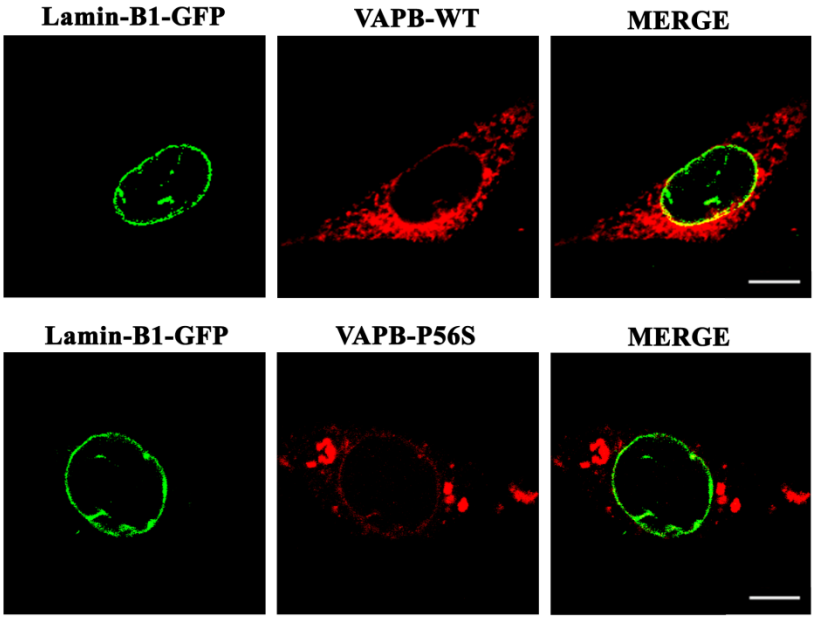

Figure 9. NE proteins are retained in mutant VAPB-containing membranes. CHO cells were co-transfected with FLAG-tagged VAPB-WT or P56S and Lamin-B1-GFP. 48 hours after transfection the cells were fixed with 4% paraformaldehyde then stained with anti-FLAG (red) and then imaged using a Zeiss LSM510 META laser scanning confocal microscope. Scale bar, 10µm.

Emerin, Pom-121, and Nup-214 are mis-localized upon siVAPB knockdown

Mutant VAPB is prone to aggregates and is thought to recruit endogenous VAPB to insoluble aggregates resulting in a dominant negative effect (Teuling et al., 2007). Cytoplasmic retention of Nups and NE proteins may be a consequence of mutant VAPB-mediated loss of endogenous VAPB function. Alternatively, cytoplasmic retention may be caused by non-specific sequestration with mutant-induced aggregates. To resolve these two possibilities, I examined the distribution of Emerin, Pom-121, an integral membrane protein anchoring the NPC with the nuclear membrane (Stavru et al., 2006), and Nup214 upon siRNA knockdown of endogenous VAPB. This should produce a phenotype similar to overexpression of VAPB-P56S if the mutant protein causes a loss of endogenous VAPB function.

CHO and HeLa cells were co-transfected with either Pom121-GFP or Nup214-GFP and with either empty lentiviral pLKO.1 vector control or with shRNA of VAPB. For the localization of Emerin, cells were co-transfected with pLKO.1 or shRNA and with monomeric RFP (mRFP) to identify the transfected cells.

Co-transfection with the empty pLKO.1 vector had no effect on the localization of Nup214-GFP, whereas siVAPB caused a relocation of Nup214-GFP to the cytoplasm and a loss from the NE (Fig. 10A). Transport of Emerin was similarly inhibited by knockdown of VAPB. Endogenous Emerin was relocated from the NE to large cytoplasmic puncta throughout the cell upon siVAPB (Fig. 10B). In the empty pLKO.1 vector expressing cells, Pom121-GFP formed a ring-like pattern of punctate spots around the NE (Fig. 10C). In contrast, Pom121-GFP was excluded from the NE and retained in large cytoplasmic puncta throughout the cell upon siVAPB (Fig. 10C). Thus, VAPB is essential for transport of these Nups to the NE.

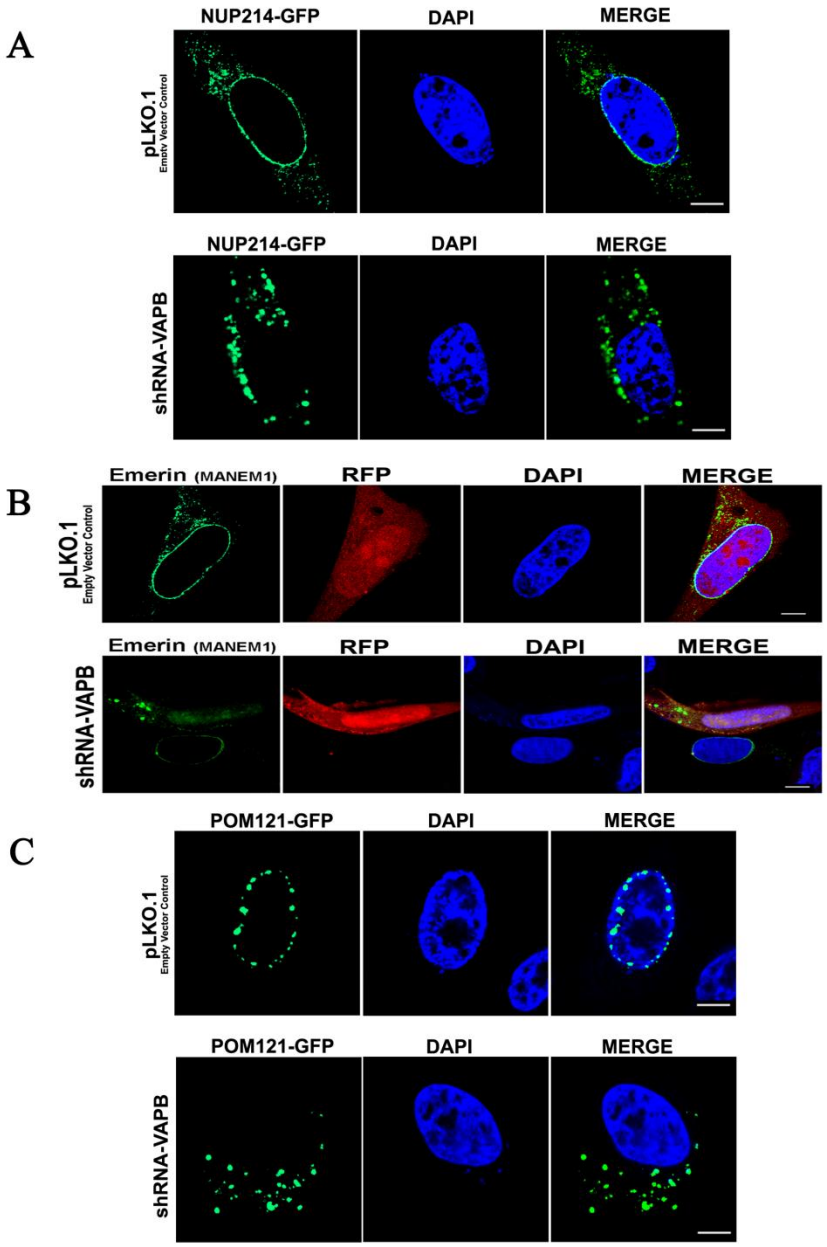

Figure 10. Cytoplasmic retention of Nup214-GFP, Emerin, and Pom121-GFP upon siVAPB knockdown. (A) HeLa cells were co-transfected with Nup214-GFP and Lentiviral constructs (empty pLKO.1 or shVAPB 152888). Forty-eight hours after transfection the cells were fixed and mounted with DAPI. (B) HeLa cells were co-transfected with mRFP and empty pLKO.1 or shVAPB. Forty-eight hours after transfection cells were fixed and stained with anti-Emerin (green) and then mounted with DAPI. (C) HeLa cells were co-transfected with Pom121-GFP and empty pLKO.1 or shVAPB. Forty-eight hours after transfection the cells were fixed and mounted with DAPI. All images were taken using a Zeiss LSM510 META laser scanning confocal microscope. Scale bar, 10μm.

Characterizing the compartment in which INM and NPC proteins are retained

VAPB is localized to the ERGIC

It has been shown that anterograde ER-to-Golgi transport of VSVG is unaffected upon siVAPB knockdown (Tran et al., 2012). Since the obtained results in this thesis demonstrated that Nups and INM proteins are retained in the cytoplasm upon knockdown of VAPB, this suggests that their transport is not via anterograde routes. Therefore, I examined retrograde transport routes. To determine the cytoplasmic compartment in which Nups and NE proteins are retained in and to identify if this compartment contains VAPB, I examined an organelle of the early secretory pathway that displays retrograde movement: The Endoplasmic Reticulum Golgi Intermediate Compartment (ERGIC). To address if this compartment contains VAPB, CHO and HeLa cells were co-transfected with ERGIC-53-GFP and VAPB-WT.

Only cells with low level of VAPB expression were examined to avoid over-expression artifacts. I found that VAPB-WT co-localized extensively with ERGIC-53-GFP cytoplasmic puncta (Fig. 11). The Golgi ribbons lacked VAPB (Fig. 12); thus, VAPB resides primarily at the ERGIC. When examined with intensity correlation analysis excluding the Golgi, VAPB-WT and ERGIC-53 showed a mean Pearson's correlation of 0.73 ± 0.02 (n=20). VAPB-WT and ERGIC-53 also showed a high Mander's overlap coefficient of 0.79 ± 0.02 (n=20). These high correlations suggest that VAPB primarily resides at the ERGIC.

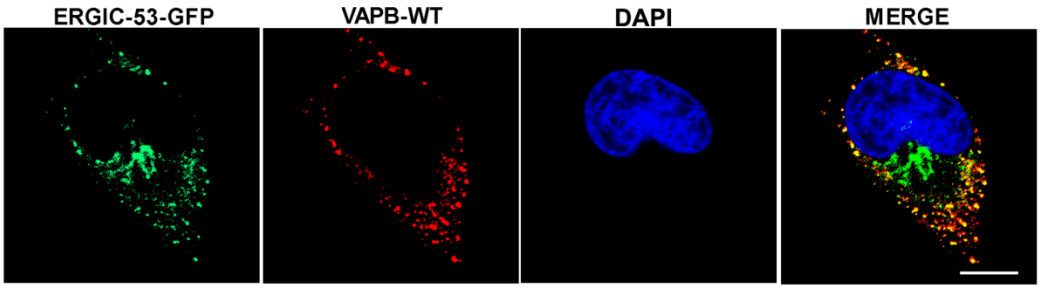

Average Pearson's Correlation Coefficient and S.E.M. VAPB-WT *(n=20)*: **+0.73 ± 0.02** Range: **+0.54 - +0.81**

Average Mander's Overlap Coefficient and S.E.M., VAPB-WT *(n=20)*: **+0.79 ± 0.02** Range: **+0.71 - +0.90**

Figure 11. VAPB is localized to the ERGIC. HeLa cells were co-transfected with VAPB-WT and GFP-ERGIC-53. Forty-eight hours after transfection, the cells were fixed with 4% paraformaldehyde in PBS for 30 min then stained with anti-FLAG (red) and mounted with DAPI. Only low expressing VAPB-WT cells were analyzed in order to eliminate possible over-expression artifacts. All images were taken using a Zeiss LSM510 META laser scanning confocal microscope. Once images were taken, the average Pearson's Correlation and Mander's Overlap Coefficients with S.E.M. was calculated to test for co-localization between VAPB-WT and ERGIC-53 using ImageJ software. A figure close to +1 indicates a positive strong co-localization between two channels. Scale bar, 10µm.

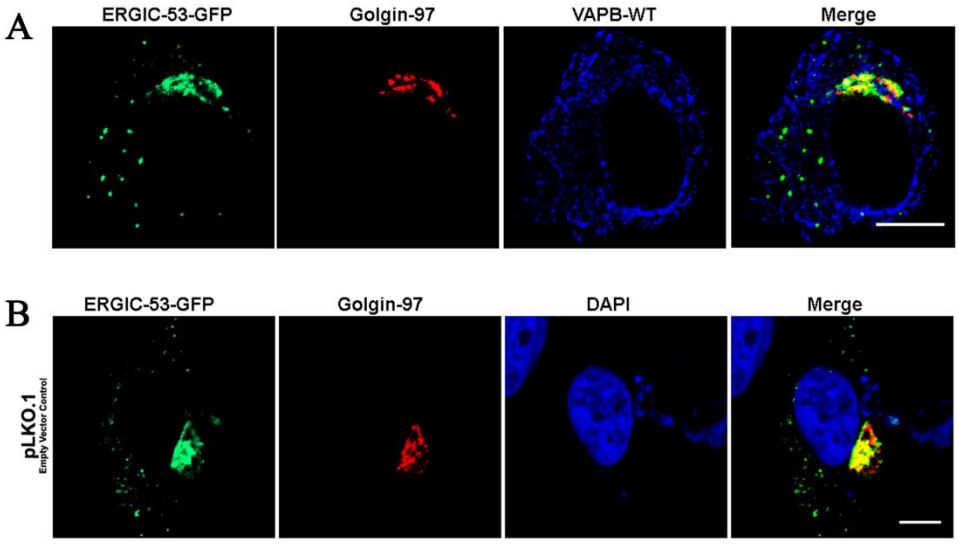

Figure 12. Immunocytochemistry of HeLa cells stained with anti-Golgin-97 towards the Golgi. (A) HeLa cells were transfected with ERGIC-53-GFP and VAPB-WT (blue). Forty-eight hours after transfection, the cells were fixed for 30 min and then stained with anti-Golgin-97 (red) to indicate Golgi localization and mounted with DAPI. (B) HelA cells were transfected with ERGIC-53-GFP and pLKO.1 empty vector control. Forty-eight hours after transfection, the cells were stained with anti-Golgin-97(red) to indicate Golgi localization and mounted with DAPI. All images were taken using a Zeiss LSM510 META laser scanning confocal microscope. Scale bar, 10 µm.

VAPB-P56S and siVAPB compromises the ERGIC

The previous results indicated that VAPB is contained in the ERGIC. Thus, I needed to address the effects of VAPB-P56S and siVAPB on the ERGIC. HeLa cells were co-transfected with ERGIC-53-GFP and VAPB-P56S or shRNA.

ERGIC-53 was localized to the Golgi complex and to scattered cytoplasmic puncta in VAPB-WT and pLKO.1 control cells but relocated to expanded membranes in VAPB-P56S and in siVAPB cells (Fig. 13A and B). Cells over-expressing VAPB-P56S were examined with intensity correlation analysis excluding the Golgi and VAPB-P56S and ERGIC-53 showed an increase in mean Pearson's correlation to 0.88 ± 0.01 (n=13) compared to VAPB-WT overexpressing cells of 0.73 ± 0.02 (n=20) (Fig. 13A). VAPB-P56S and ERGIC-53 also showed an increase in Mander's overlap coefficient to 0.93 ± 0.01 (n=13) compared to VAPB-WT over-expressing cells of 0.79 ± 0.02 (n=20) (Fig. 13A). These high correlations suggest that VAPB-P56S may induce VAPB to be retained highly at the ERGIC.

The expanded ERGIC membranes seen in P56S and the siVAPB were seen in 36% of cells compared to 4% in control cells (Fig. 14). Further, I quantified, using Feret's diameter, the size of the expanded ERGIC aggregates seen in siVAPB and VAPB-P56S transfected cells (Fig. 15). Empty pLKO.1 cells had an average diameter of 167.6 nm ± 4.95 (n=538) (Fig. 15A). In contrast, knockdown cells showed a significant increase in expansion at 515.1 nm ± 22.68 (n=1113) (Fig. 15A). In empty vector cells the average size of the punctate clusters seen with ERGIC-53 was 174.5 nm ± 8.06 (n=199) (Fig. 15B). This is similar to VAPB-WT cells at 144.2 nm ± 2.53 (n=1092) (Fig. 15B). In contrast, VAPB-P56S transfected cells show expanded clusters at a significant increase to 353 nm ± 23.25 (n=91) (Fig. 15B). Thus, cells transfected with either VAPB-P56S or shVAPB exhibit an expansion in the diameter of the ERGIC.

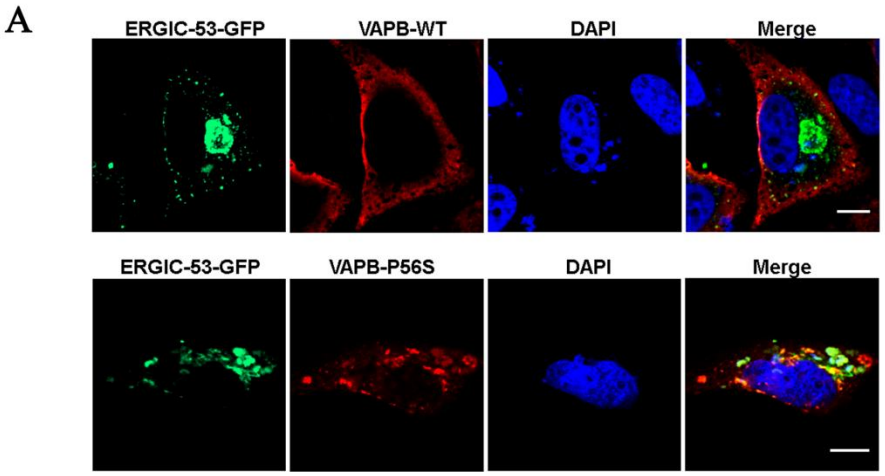

Average Pearson's Correlation Coefficient and S.E.M. VAPB-P56S *(n=13)*: **+0.88 ± 0.01** Range: **+0.81 - +0.95**

Average Mander's Overlap Coefficient and S.E.M., VAPB-P56S *(n=13)*: **+0.93 ± 0.01** Range: **+0.82 - +0.96**

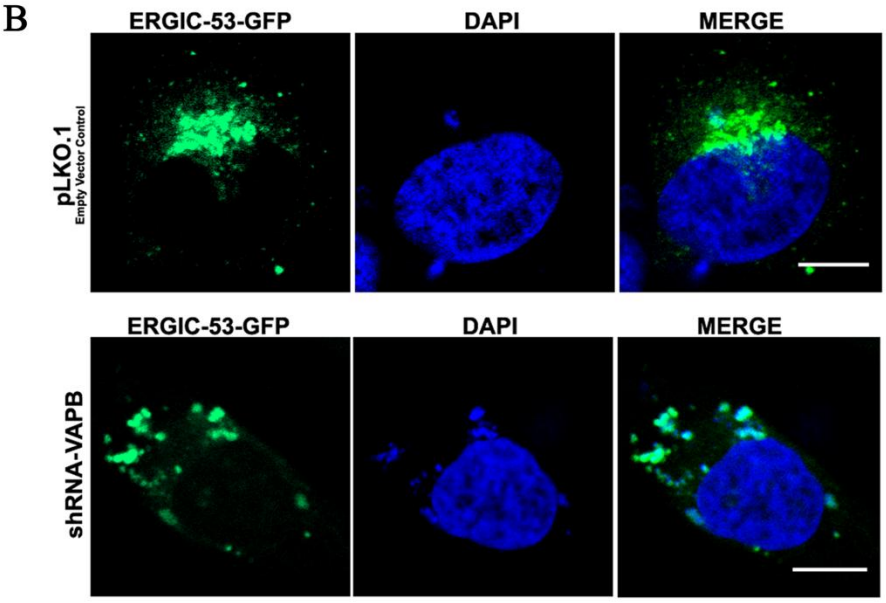

Figure 13. The ERGIC is compromised in the presence of VAPB-P56S and with shVAPB.
(A) HeLa Cells were co-transfected with GFP-ERGIC-53 and FLAG-tagged VAPB-WT or P56S. Forty-eight hours after transfection, the cells were fixed with 4% paraformaldehyde in PBS for 30 min and then stained with anti-FLAG (red) and mounted with DAPI. (B) HeLa cells were co-transfected with GFP-ERGIC-53 and empty pLKO.1 or siVAPB. Forty-eight hours after transfection, the cells were fixed and then mounted with DAPI. All images were taken using a Zeiss LSM510 META laser scanning confocal microscope. Once images were taken, the average Pearson's Correlation and Mander's Overlap Coefficients with the S.E.M. was calculated to test for co-localization between VAPB-P56S and ERGIC-53-GFP using ImageJ software for (A). A +1 figure indicates a strong positive correlation between two channels. Scale bar, 10μm.

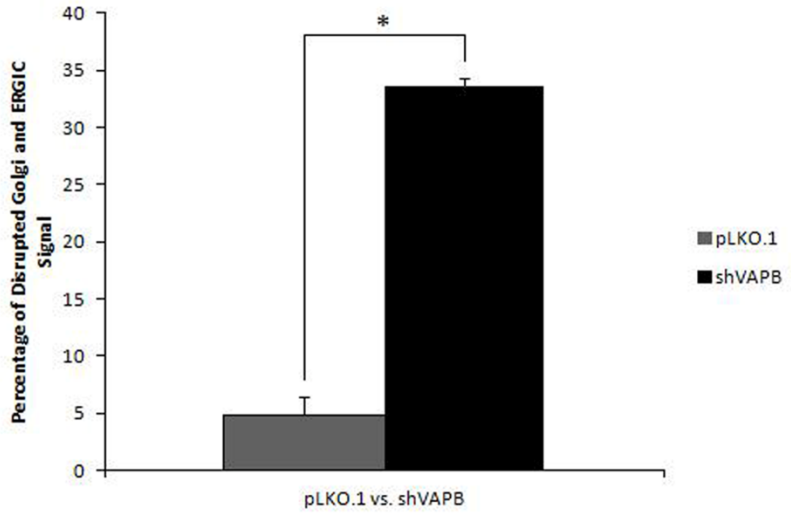

Figure 14. P56S induces an expanded and disrupted ERGIC. Hela cells were co-transfected with ERGIC-53-GFP and either pLKO.1 empty vector or shVAPB. Forty-eight hours after transfection, the cells were fixed with 4% paraformaldehyde and then mounted with DAPI. All images were taken using a Zeiss LSM510 META laser scanning confocal microscope. Once images were taken, an average of 200 cells were counted for each condition. The values obtained represent the % of HeLa cells containing ERGIC expanded aggregates ± S.E.M., n=3. Statistical analysis comparing pLKO.1 to shVAPB expressing cells was performed using a *Student t-test. $P<0.05$.

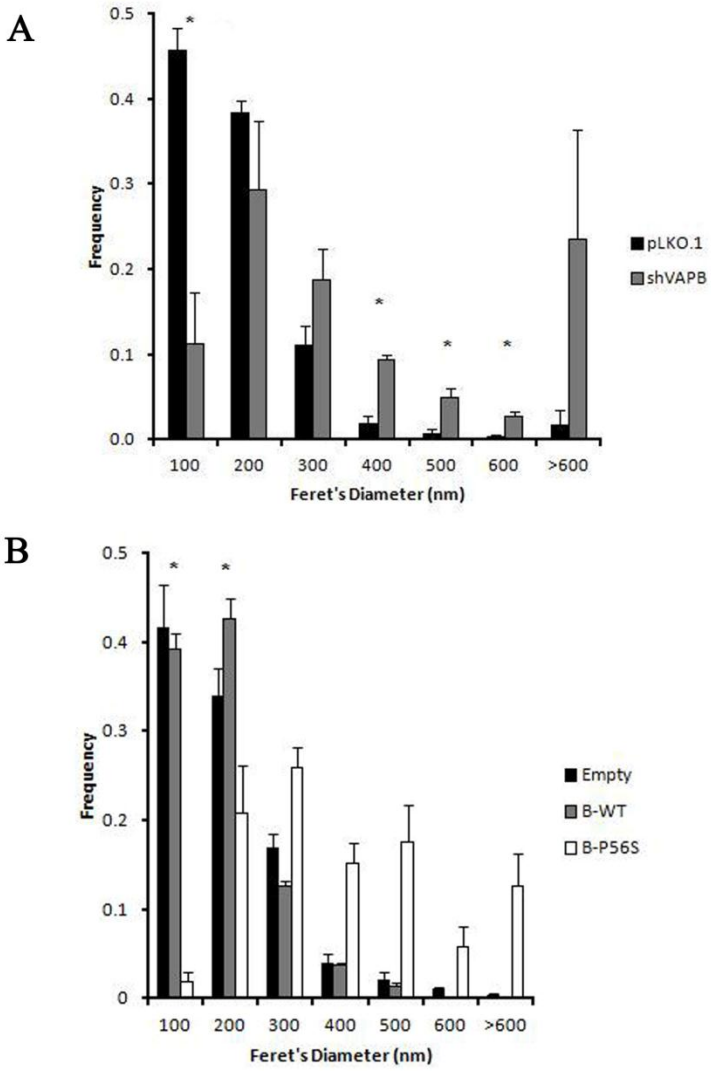

Figure 15. The ERGIC is expanded in the presence of VAPB-P56S and shVAPB. (A) HeLa cells were co-transfected with GFP-ERGIC-53 and pLKO.1 or shVAPB. Forty-eight hours after transfection, the cells were fixed and mounted with DAPI. Images were collected on a Zeiss LSM510 META laser scanning confocal microscope. Once images were collected, 538 ERGIC puncta signal was measured by their diameter in nm for pLKO.1 control cells and 1113 for shVAPB. Values are represented as the frequency of HeLa cells containing ERGIC of a given diameter in nm ± S.E.M., n=3. (B) HeLa cells were co-transfected with GFP-ERGIC-53 and empty vector or VAPB-WT or VAPB-P56S. Forty-eight hours after transfection, the cells were fixed and stained with anti-FLAG (red) and then mounted with DAPI. Once images were collected using a Zeiss LSM510 META laser scanning confocal microscope, 199 ERGIC puncta signal were measured for the empty control, 1092 for the WT and 91 for P56S. Values are represented as the frequency of HeLa cells containing ERGIC of a given diameter in nm ± S.E.M., n=3. Statistical analysis comparing pLKO.1 to shVAPB and empty to WT and P56S expressing cells was performed using a *Student t-test. $P<0.05$.

The ERGIC distortion is not due to over-expression of ERGIC-53

To eliminate the possibility that the ERGIC expansion may be due to over-expression of ERGIC-53, the previous experiments were repeated with an antibody towards the ERGIC. HeLa cells were transfected with VAPB-WT or VAPB-P56S. Forty-eight hours later, cells were fixed and stained with anti-ERGIC-53/p58 (green) a polyclonal antibody produced in rabbit and FLAG-tagged VAPB (red). Later, the cells were imaged using a confocal microscope. For the siRNA group, HeLa cells were co-transfected with mRFP and either pLKO.1 or shRNA and then stained with the ERGIC antibody.

In accordance with the previous experiment, only cells with low level of expression of transfected VAPB were examined. I found that VAPB-WT co-localized extensively with ERGIC-53 antibody cytoplasmic puncta (Fig. 16A). When subjected to intensity correlation analysis excluding the Golgi, VAPB-WT and ERGIC-53 showed a mean Pearson's correlation of 0.75 ± 0.03 (n=23) and a Mander's overlap coefficient of 0.76 ± 0.02 (n=23) (Fig. 16A). The VAPB-P56S mutation causes an increase in the Pearson's correlation to 0.85 ± 0.03 (n=10) and an increase in Mander's overlap coefficient of 0.86 ± 0.02 (Fig. 16B).

ERGIC was primarily localized to the Golgi with cytoplasmic clusters in pLKO.1 and VAPB-WT cells. In contrast, ERGIC was relocated to expanded membranes in siVAPB cells and this may also be the case in VAPB-P56S cells (Fig. 16C). The expanded membranes were measured by Feret's Diameter (Fig. 17). pLKO.1 cells had an average ERGIC membrane diameter of 86.35 nm ± 3.42 (n=374). In contrast, siRNA knockdown cells showed a significant membrane diameter increase to 167.5 nm ± 11.75 (n=193) (Fig. 17A). Empty vector cells had an average membrane diameter of 69.23 nm ± 1.52 (n=770) similar to VAPB-WT cells at 80.11 nm ± 3.12 (n=438). In contrast, VAPB-P56S cells show a significant increase in diameter to 221 nm ± 17.33 (n=118) (Fig. 17B).

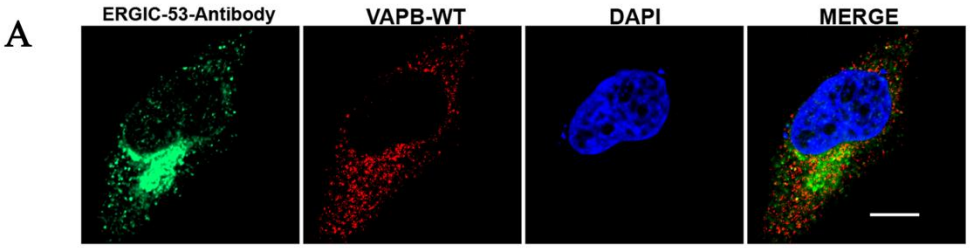

Average Pearson's Correlation Coefficient and S.E.M. VAPB-WT *(n=23)*: **+0.75 ± 0.03** Range: **+0.41 - +0.89**

Average Mander's Overlap Coefficient and S.E.M., VAPB-WT *(n=23)*: **+0.76 ± 0.02** Range: **+0.54 - +0.91**

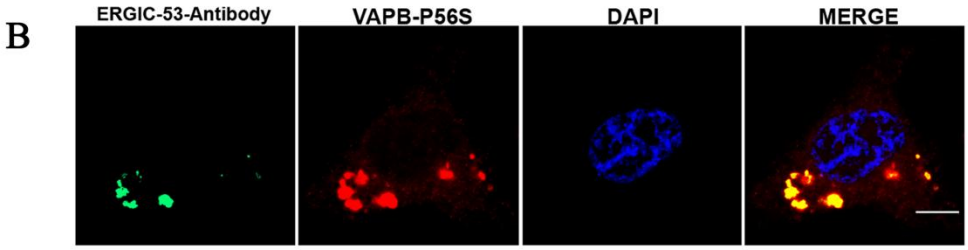

Average Pearson's Correlation Coefficient and S.E.M. VAPB-P56S *(n=10)*: **+0.85 ± 0.03** Range: **+0.72 - +0.96**

Average Mander's Overlap Coefficient and S.E.M., VAPB-P56S *(n=10)*: **+0.86 ± 0.02** Range: **+0.64 - +0.95**

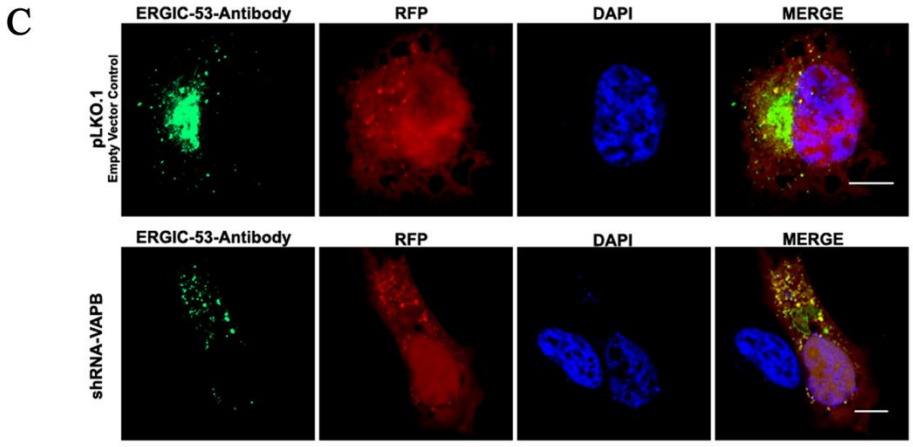

Figure 16. The ERGIC distortion is not an over-expression effect. (A) HeLa cells were transfected with VAPB-WT. Forty-eight hours after transfection, the cells were fixed and stained with anti-FLAG (red) and anti-ERGIC-53/p58 then mounted with DAPI. Only low expressing VAPB-WT cells were examined to avoid overexpression artifacts. (B) HeLa cells were transfected with VAPB-P56S. Forty-eight hours after transfection, the cells were fixed and stained with anti-FLAG (red) and anti-ERGIC-53/p58 (green) then mounted with DAPI. The average Pearson's Correlation and Mander's Overlap Coefficients with the S.E.M. was calculated to quantify the correlation between the ERGIC and VAPB-WT or VAPB-P56S using ImageJ software. A value of +1 indicates a strong positive correlation between two channels. (C) HeLa cells were co-transfected with mRFP and empty pLKO.1 or shVAPB. Forty-eight hours after transfection, thc cells were fixed and then stained with and anti-ERGIC-53/p58 (green) and mounted with DAPI. Scale bar, 10µm.

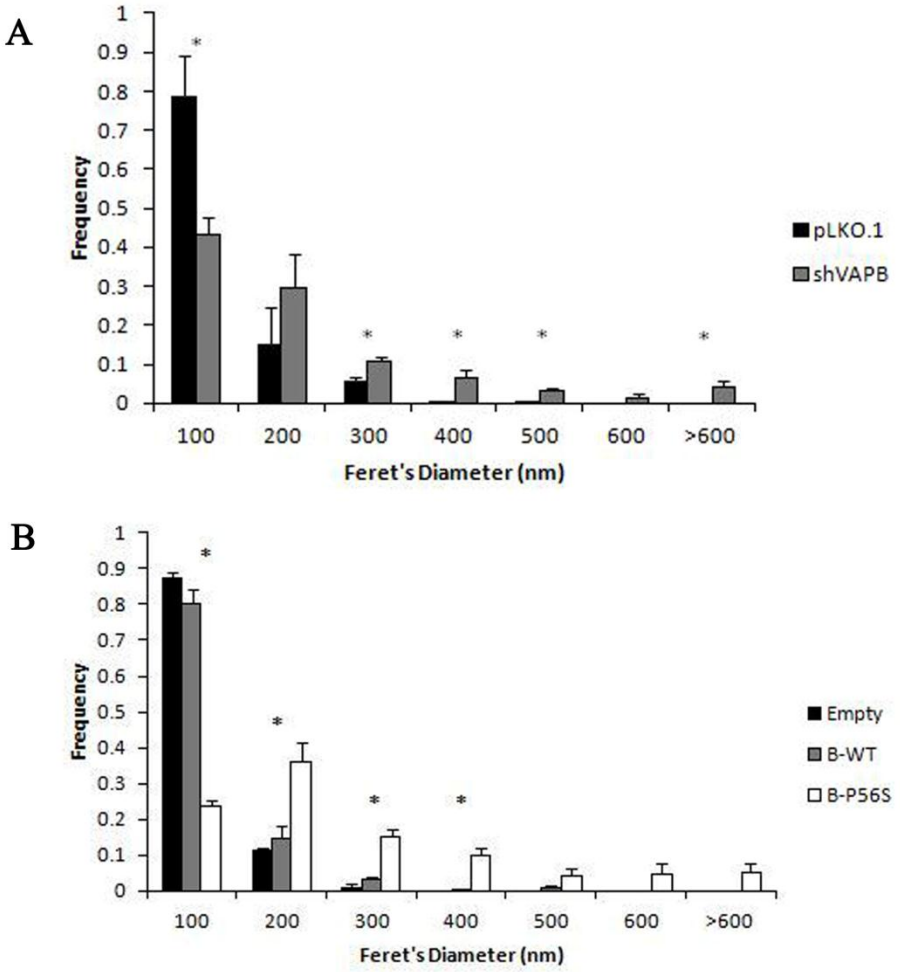

Figure 17. Endogenous ERGIC is expanded in the presence of VAPB-P56S and shVAPB. (A) HeLa cells were co-transfected with mRFP and pLKO.1 or shVAPB. Forty-eight hours after transfection, the cells were fixed and stained with anti-ERGIC-53/p58 (green). Upon collecting images using a Zeiss LSM510 Meta laser scanning confocal microscope, 374 clusters of ERGIC were measured by their diameter in nm for pLKO.1 control cells and 193 for shVAPB. Values are represented as the frequency of HeLa cells containing ERGIC of a given diameter in nm ± S.E.M., n=3. (B) HeLa cells were transfected with empty vector or VAPB-WT or VAPB-P56S. Forty-eight hours after transfection, the cells were fixed and then stained with anti-FLAG (red) and anti-ERGIC-53/p58 (green). After the collection of the images, 770 clusters of ERGIC were measured by their diameter (nm) for empty control, 438 for the WT and 118 for P56S. Values are represented as the frequency of HeLa cells containing ERGIC of a given diameter in nm ± S.E.M., n=3. Statistical analysis comparing pLKO.1 to shVAPB and Empty to WT and P56S expressing cells was performed using a *Student t-test. $P<0.05$.

Emerin, Mab414 and Nup214-RFP Co-localize with ERGIC-53

Previous results indicated that VAPB co-localized with the ERGIC. The results also indicated that the ERGIC is expanded in the presence of P56S and upon siRNA knockdown of endogenous VAPB. I hypothesize that the expansion may be the result of accumulated proteins transported to and retained at the ERGIC due to loss of VAPB retrograde transport. To address if Nups are transported to the ERGIC, I co-transfected cells with either pLKO.1 and ERGIC-53-GFP and stained for Mab414 or for Emerin or co-transfected cells with Nup214-RFP to undergo a correlation analysis with ERGIC-53.

ERGIC-53 primarily resides at the Golgi (Fig. 12); however, there are punctate inclusions located in the cytoplasm. These punctate inclusions are believed to be the ERGIC where proteins are transported. Emerin, Nup214 and Mab414 were tested to see if they co-localized with these punctate inclusions in the cytoplasm. When subjected to intensity correlation analysis excluding the Golgi, Emerin and ERGIC-53 showed an average Pearson's correlation coefficient of 0.49 ± 0.02 (n=24) and a Mander's overlap coefficient of 0.68 ± 0.02 (n=24) (Fig. 18A). Nup214-RFP average a Person's correlation coefficient of 0.47 ± 0.04 (n=18) and a Mander's overlap coefficient of 0.79 ± 0.03 (n=18) (Fig. 19A). Lastly, Mab414 averaged a Pearson's correlation coefficient of 0.57 ± 0.04 (n=17) and a Mander's overlap coefficient of 0.73 ± 0.03(n=17) (Fig. 20A). These figures indicate that NE proteins and Nups are transported to the ERGIC via vesicular transport prior to the NE.

Furthermore, the ERGIC-53-GFP, Emerin and Mab414 punctate inclusions in the cytoplasm were measured by their Feret's diameter in nm for pLKO.1 control expression cells. Punctate inclusion that were stained specifically with endogenous Emerin had an average diameter of 100.8 nm ± 1.68 (n=1524) (Fig. 21A). Mab414 stained pLKO.1 control cells had cytoplasmic inclusions with

an average diameter of 128 nm ± 2.3 (1683) (Fig. 21B). These figures are very close the normal diameter of the ERGIC compartment previously examined under VAPB-WT and ERGIC-53 conditions (see Fig. 15 or 17).

Emerin, Mab414 and Nup-214 are retained at the ERGIC upon shVAPB

The previous results indicated that certain Nups and INM proteins are transported to the ERGIC. This raised the question: Can this be the compartment in which the proteins are retained in because of the loss of VAPB? To verify that Nups are retained at the ERGIC in a VAPB-dependent manner, I stained VAPB knockdown cells with Emerin or Mab414 or co-transfected cells with Nup214-RFP to determine if these proteins are retained at the expanded ERGIC membranes.

Emerin is localized to the NE and had small cytoplasmic puncta in control cells, but is relocated to the expanded ERGIC along with ERGIC-53 in siVAPB cells (Fig. 18B). When subjected to intensity correlation analysis excluding the Golgi, Emerin and ERGIC-53 showed an average Pearson's correlation coefficient of 0.89 ± 0.01 (n=30) and a Mander's overlap coefficient of 0.91 ± 0.01 (n=30) (Fig. 18B). Nup214 was also seen in small cytoplasmic puncta in control cells and localized to the NE, but was relocated to the expanded ERGIC upon siVAPB (Fig. 19B). Nup214-RFP averaged a Pearson's correlation coefficient of 0.88 ± 0.01 (n=21) and a Mander's overlap coefficient of 0.94 ± 0.01 (n=21) (Fig. 19B). Mab414 was localized to the rim of the NE and in small cytoplasmic puncta in control cells, but was retained in expanded ERGIC-containing membranes upon siVAPB (Fig. 20B). Mab414 averaged a Pearson's correlation of 0.79 ± 0.02 (n=14) and a Mander's overlap coefficient of 0.83 ± 0.01 (n=14) (Fig. 20B). Emerin, Nup214 and Mab414 all showed an increase in correlation with the ERGIC upon knockdown of endogenous VAPB compared to control cells. Thus, NE proteins and Nups transit through the ERGIC and are retained in the ERGIC resulting in the accumulation of proteins, the expansion of the ERGIC and

an increase in correlation. VAPB is essential in NE and NPC protein transport to the NE.

Furthermore, under knockdown of endogenous VAPB the ERGIC-53-GFP, Emerin and Mab414 punctate inclusions in the cytoplasm illustrated a shift towards larger ERGIC-53 puncta based on their Feret's diameter. Punctate inclusion that were stained specifically with endogenous Emerin under shVAPB conditions had an average diameter of 191.17 nm ± 3.98 (n=1206) compared to control cells with 100.8 nm ± 1.68 (n=1524) (Fig. 21A). Mab414 stained shVAPB control cells averaged a diameter of cytoplasmic inclusions of 182.62 nm ± 5.09 (n=825) compared to control cells with 128 nm ± 2.3 (1683) (Fig. 21B). These figures are very close the expanded diameter obtained previously under VAPB-P56S or shVAPB and ERGIC-53 conditions (see Fig. 15 or 17). Thus, quantitation of Emerin and Mab414 cytoplasmic puncta indicated a shift towards larger puncta in knockdown cells (Fig. 21). Together, this indicates that NE and transmembrane Nups transit through ERGIC, and VAPB is required for final transport to the NE.

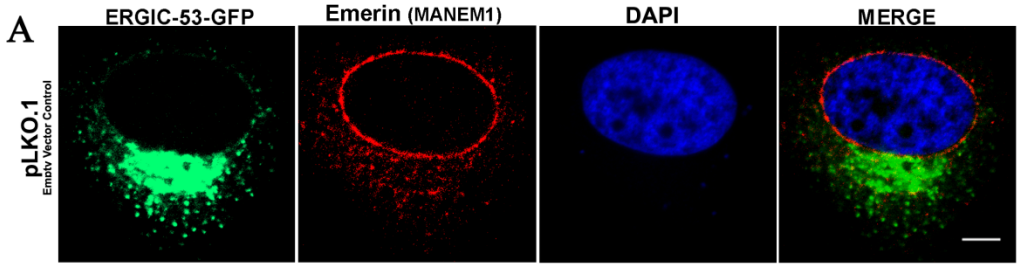

Average Pearson's Correlation Coefficient and S.E.M., *(n=24)*: **+0.49 ± 0.02** Range: **+0.31 - +0.74**

Average Mander's Overlap Coefficient and S.E.M., *(n=24)*: **+0.68 ± 0.02** Range: **+0.79 - +0.88**

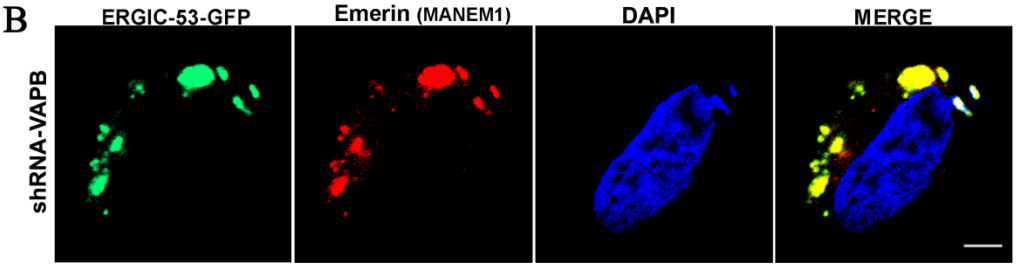

Average Pearson's Correlation Coefficient and S.E.M., *(n=30)*: **+0.89 ± 0.01** Range: **+0.73 - +0.97**

Average Mander's Overlap Coefficient and S.E.M., *(n=30)*: **+0.91 ± 0.01** Range: **+0.78 - +0.98**

Figure 18. NE Proteins and NPC Proteins are localized to the ERGIC. (A) HeLa cells were co-transfected with GFP-ERGIC-53 and empty pLKO.1. Forty-eight hours after transfection, the cells were fixed with 4% paraformaldehyde for 30 min, stained with anti-Emerin antibody and then mounted with DAPI. (B) HeLa cells were co-transfected with GFP-ERGIC-53 and siVAPB. Forty-eight hours after transfection, the cells were fixed and stained with anti-Emerin antibody and mounted with DAPI. The average Pearson's Correlation and Mander's Overlap Coefficients with the S.E.M. was calculated for both (A) and (B) in order to quantify the correlation between the ERGIC compartment and Emerin. A figure of +1 represents a strong positive correlation between two channels. Scale bar, 10μm.

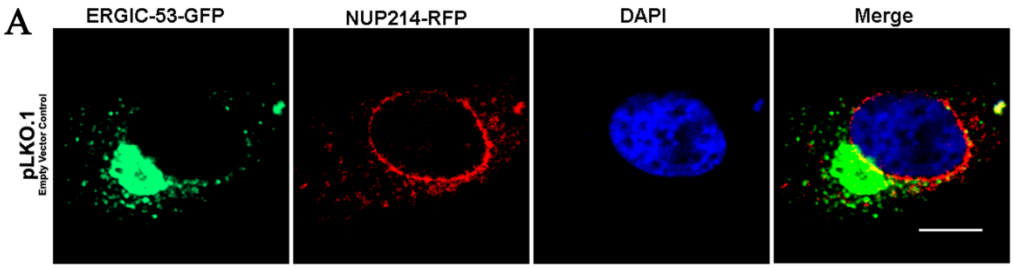

Average Pearson's Correlation Coefficient and S.E.M., *(n=18)*: **+0.47 ± 0.04** Range: **+0.18 - +0.75**

Average Mander's Overlap Coefficient and S.E.M., *(n=18)*: **+0.79 ± 0.03** Range: **+0.54 - +0.94**

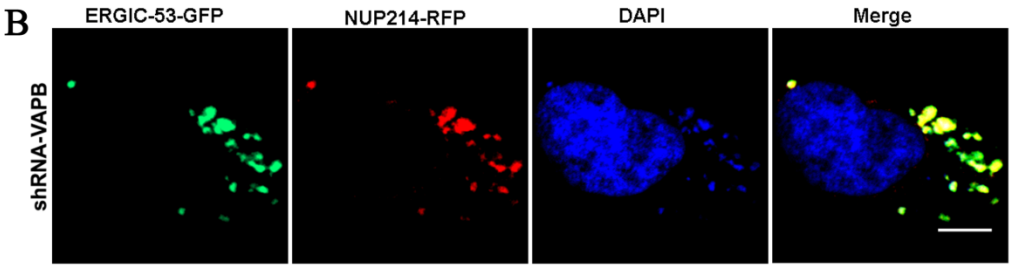

Average Pearson's Correlation Coefficient and S.E.M., *(n=21)*: **+0.88 ± 0.01** Range: **+0.76 - +0.94**

Average Mander's Overlap Coefficient and S.E.M., *(n=21)*: **+0.94 ± 0.01** Range: **+0.87 - +0.98**

Figure 19. NE Proteins and NPC Proteins are localized to the ERGIC. (A) HeLa cells were co-transfected with GFP-ERGIC-53, Nup214-RFP and empty pLKO.1. Forty-eight hours after transfection, the cells were fixed with 4% paraformaldehyde for 30 min and then mounted with DAPI. (B) HeLa cells were co-transfected with GFP-ERGIC-53, Nup214-RFP and siVAPB. Forty-eight hours after transfection, the cells were fixed and then mounted with DAPI. The average Pearson's Correlation and Mander's Overlap Coefficients with the S.E.M. was calculated for both (A) and (B) in order to quantify the correlation between the ERGIC compartment and Nup214. A figure of +1 represents a strong positive correlation between two channels. Scale bar, 10µm.

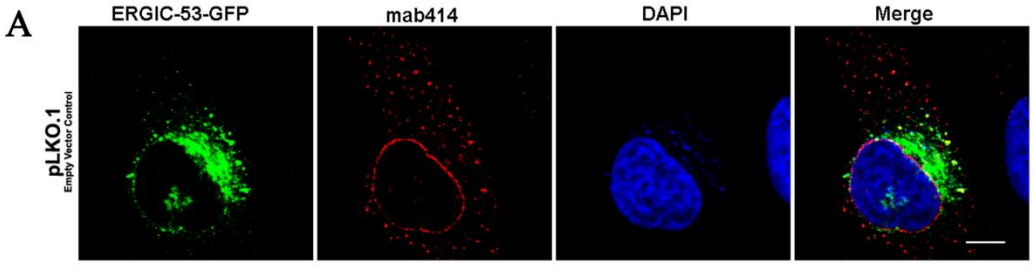

Average Pearson's Correlation Coefficient and S.E.M., *(n=17)*: **+0.57 ± 0.04** Range: **+0.33 - +0.76**

Average Mander's Overlap Coefficient and S.E.M., *(n=17)*: **+0.73 ± 0.03** Range: **+0.48 - +0.89**

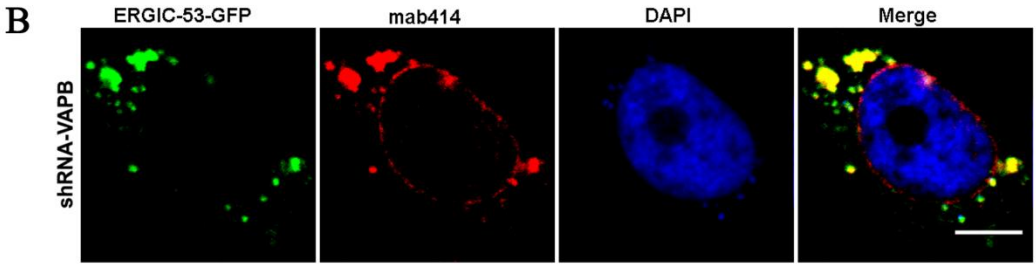

Average Pearson's Correlation Coefficient and S.E.M., *(n=14)*: **+0.79 ± 0.02** Range: **+0.62 - +0.91**

Average Mander's Overlap Coefficient and S.E.M., *(n=14)*: **+0.83 ± 0.01** Range: **+0.72 - +0.92**

Figure 20. NE Proteins and NPC Proteins are localized to the ERGIC. (A) HeLa cells were co-transfected with GFP-ERGIC-53 and empty pLKO.1. Forty-eight hours after transfection, the cells were fixed with 4% paraformaldehyde for 30 min, stained with anti-mab414 antibody which recognizes FG repeat Nup and then mounted with DAPI. (B) HeLa cells were co-transfected with GFP-ERGIC-53 and siVAPB. Forty-eight hours after transfection, the cells were fixed then stained with anti-mab414 antibody and then mounted with DAPI. The average Pearson's Correlation and Mander's Overlap Coefficients with the S.E.M. was calculated for both (A) and (B) in order to quantify the correlation between the ERGIC compartment and Mab414 staining. A figure of +1 illustrates a strong positive correlation between two channels. Scale bar, 10μm.

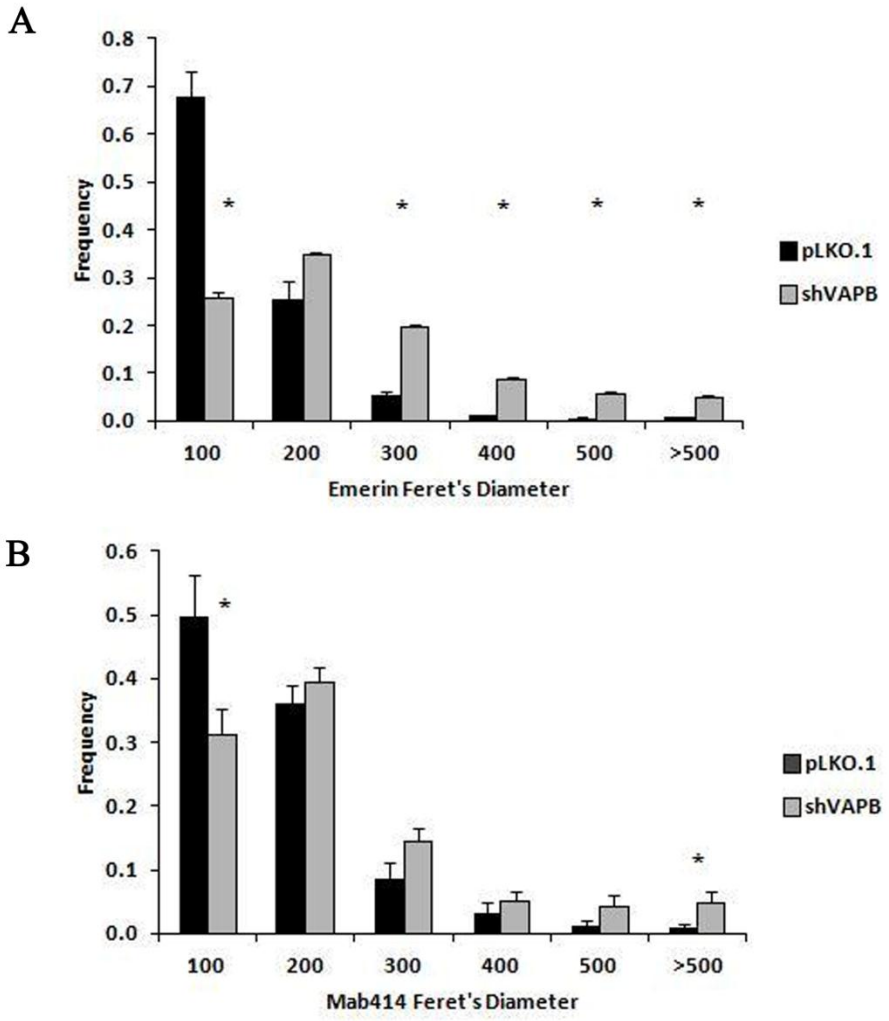

Figure 21. Endogenous Emerin and Mab414 are retained in expanded ERGIC upon knockdown of VAPB. (A) HeLa cells were co-transfected with ERGIC-53-GFP and pLKO.1 or shVAPB. Forty-eight hours after transfection, the cells were fixed with 4% paraformaldehyde in PBS for 30 min then stained for endogenous Emerin with MANEM1 and mounted with DAPI. (B) HeLa cells were co-transfected with ERGIC-53-GFP and pLKO.1 or shVAPB. Forty-eight hours after transfection, the cells were fixed then stained with mab414 antibodies and then mounted with DAPI. For both (A) and (B) images were collected using a Zeiss LSM510 Meta laser scanning confocal microscope. Once images were generated, the Feret's diameter of the cytoplasmic puncta of the ERGIC and either the Emerin or Mab414 signal was calculated. The values are represented in a distribution histogram of Feret's diameter of cytoplasmic puncta in 100 nm bins for Emerin and mab414 ± S.E.M., n=3. Statistical analysis comparing pLKO.1 to shVAPB exressing cells was performed using a *Student t-test. $P<0.05$.

ERGIC-53 Accumulates in the ERGIC at 15°C and Retains Emerin

Incubation at 15°C is known to reversibly accumulate ERGIC-53 in the ERGIC by blocking retrograde transport to the ER (Hauri et al., 2000; Ben-Tekaya et al 2005). Thus, I hypothesize that if NE proteins are transported via vesicular transport to the ERGIC and then to the NE, NE proteins will be retained in expanded ERGIC membranes due to lack of retrograde transport at 15°C. Cells were transfected with ERGIC-53-GFP and forty-eight hours later were transferred from 37°C to 15°C from 0-8 hours. At each hour, cells were fixed and stained for endogenous emerin. Since the ERGIC will expanded at 15°C, I propose that Emerin should be retained at the ERGIC.

In control cells at time 0 hours and 37°C, ERGIC-53 localized to the Golgi and in punctate staining throughout the cytoplasm. Emerin formed a ring-like pattern along the NE (Fig. 22). In contrast, at 15°C for 4 hours, Emerin was retained in dilated cytoplasmic membranes and excluded from the NE (Fig. 22). The ERGIC was also seen to lose the cytoplasmic puncta throughout the cell and formed expanded membrane compartments in the cytoplasm that also contained Emerin (Fig. 22). This suggests that Emerin is transported from the ER to the ERGIC and then to the NE by vesicular transport that requires VAPB.

This set of data illustrates Emerins transport route independent of VAPB-P56S and knockdown of endogenous VAPB effects. This clearly depicts that Emerin is transported to the ERGIC before the NE. Due to the loss of retrograde transport at 15°C, Emerin is retained at the ERGIC. Thus, VAPB-P56S or shVAPB loss of VAPB retrograde transport may be the reason why Emerin is trapped at the ERGIC.

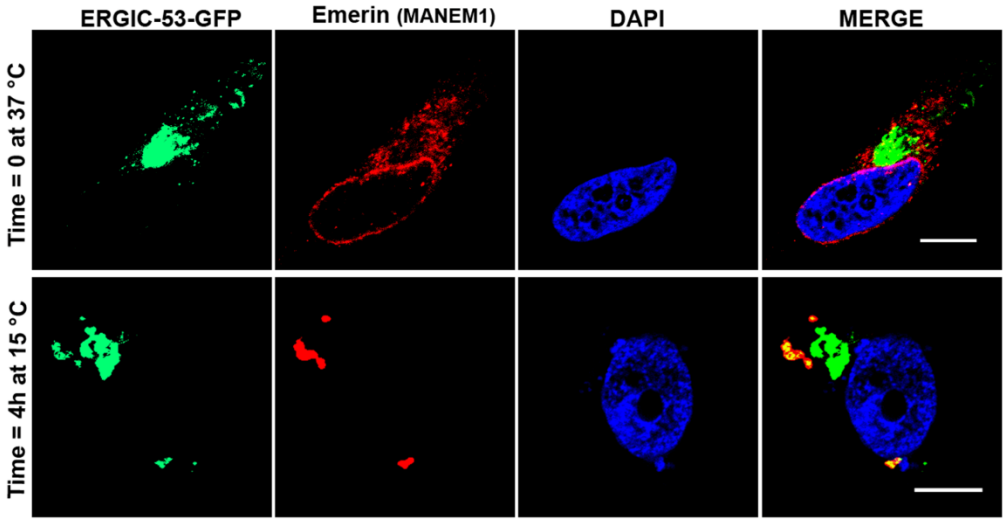

Figure 22. ERGIC-53 accumulates in the ERGIC at 15°C and retains Emerin in this compartment. HeLa cells were transfected with GFP-ERGIC-53. Forty-eight hours later, cells were transferred from 37°C to 15°C in order to block retrograde transport from the ERGIC and trap ERGIC-53 in the ERGIC. Once each sample was collected each hour, the cells were fixed with 4% paraformaldehyde then stained with anti-MANEM1 towards endogenous Emerin and then mounted with DAPI. Images were collected using a Zeiss LSM510 Meta laser scanning confocal microscope. Time 0 represents cells that were fixed and stained with anti-Emerin antibody at 37°C. Time 4 hours represents cells that were fixed and stained with anti-Emerin antibody at 15°C. Scale bar, 10µm.

Consequence of a Defective NE and NPC Assembly

VAPB-P56S causes a delay in nuclear translocation of activated GR and the FFAT motif rescues the delay

I utilized a ligand-activated Glucocorticoid Receptor (GR) to examine if the VAPB-P56S induced altered NPC composition might have an effect on nucleocytoplasmic shuttling. GR normally resides in the cytoplasm, and is imported into the nucleus upon binding to glucocorticoid agonist Dexamethasone (Dex). CHO cells were transfected with GFP-tagged GR and either empty vector control, VAPB-WT or VAPB-P56S. Forty-eight hours after transfection, cells were incubated in serum-free medium for 2 hours. Subsequently, 1µm of Dex was added and cells were fixed at 15 minute intervals up to 1 hour. The nuclear fluorescence was quantified as a percentage of total cellular fluorescence, and a threshold value of ≥60% was used to indicate nuclear import. I also performed another set of experiments co-transfecting cells with the FFAT motif.

At 15 min Dex treatment, empty FLAG and VAPB-WT transfected cells exhibited nuclear GR in 80% ± 13% and 85% ± 9% (n=3) of the cell population, respectively (Fig. 23A and C). In contrast, nuclear localization of GR-GFP was significantly lowered in mutant VAPB transfected cells with only 32% ± 5% of transfected cells exhibiting nuclear GR-GFP at 15 min and 44% ± 5% at 30 min (Fig. 23B and C). GR-GFP was eventually translocated to the nucleus at 45 and 60 min intervals, indicating nuclear import was significantly delayed but not completely blocked in these cells (Fig. 23B and C). Simultaneous overexpression of FFAT with VAPB-P56S restored the import delay and did not have any effect on VAPB-WT (Fig. 24 A, B and C); suggesting VAPB-P56S-induced changes in the NE are the likely cause of the delay.

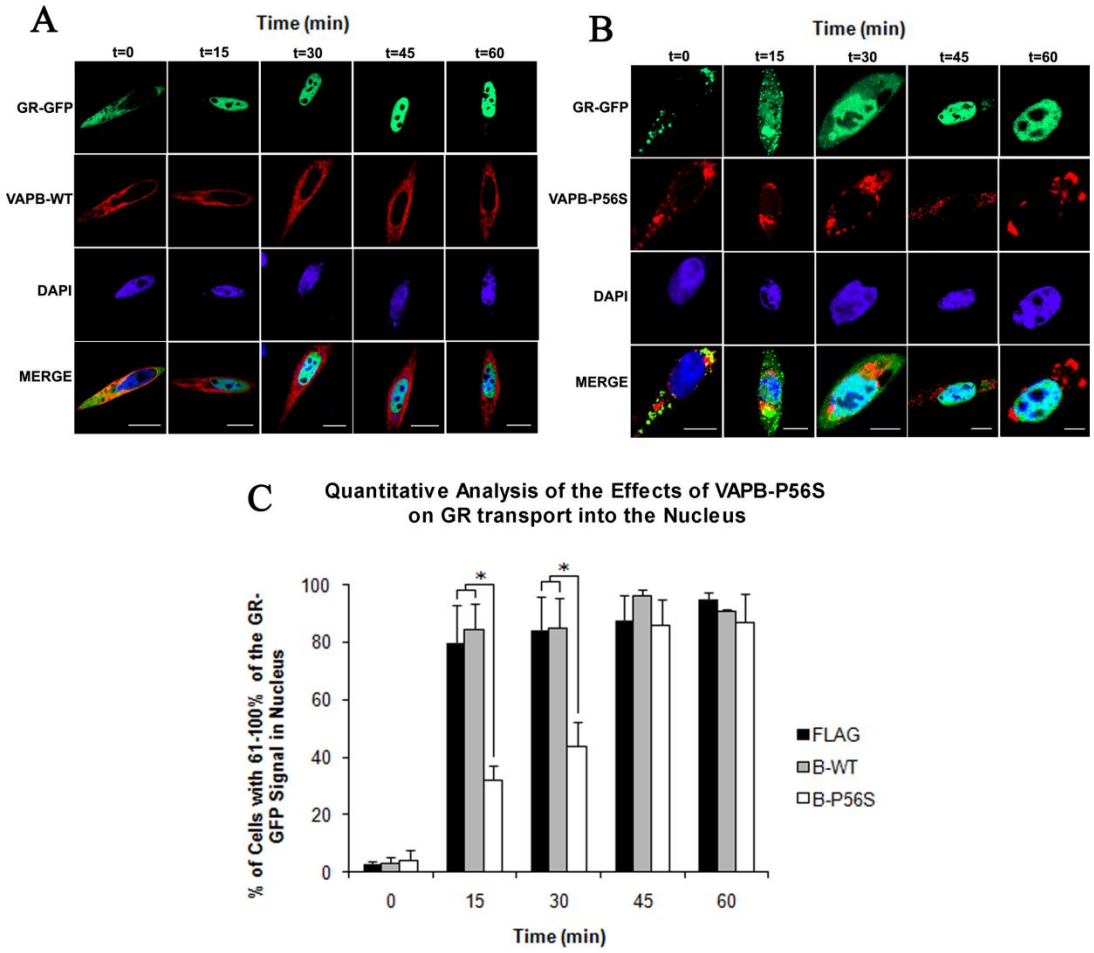

Figure 23. VAPB-P56S causes a time delay in nuclear translocation of activated GR. (A) CHO cells were co-transfected with VAPB-WT and GR-GFP. Forty-eight hours after transfection, 1µm of dexamethasone was administered and cells were fixed every 15 minutes for one hour and then stained with anti-FLAG (red) and mounted with DAPI. (B) CHO cells were co-transfected with VAPB-P56S and GR-GFP and treated as in (A). (C) An average of 86 cells was quantified for each condition. Values are represented as % of CHO cells containing 61-100% of the GR-GFP signal in the nucleus at each specific time point ± S.E.M. n=3. Statistical analysis comparing FLAG or VAPB-WT to VAPB-P56S expressing cells were performed using a Student t-test, $p<0.05$*. Scale bar, 10µm.

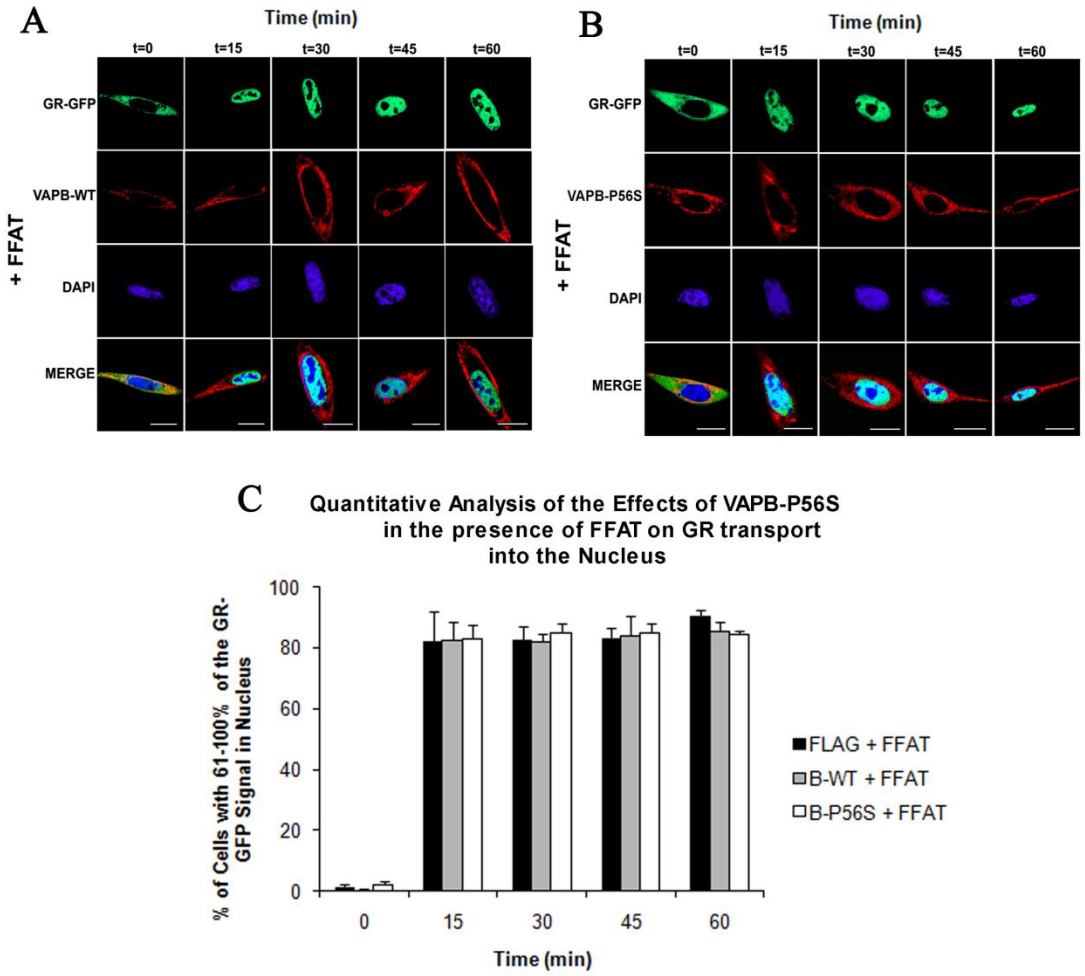

Figure 24. The FFAT motif restores proper nuclear translocation of GR. CHO cells were co-transfected with VAPB-WT (A) or VAPB-P56S (B), GR-GFP and the FFAT motif of rabbit OSBP. Forty-eight hours after transfection, 1µm of dexamethasone was administered and cells were fixed every 15 minutes for one hour then stained with anti-FLAG (red) and then mounted with DAPI. (C) An average of 68 cells was quantified for each condition. Values are represented as % of CHO cells containing 61-100% of the GR-GFP signal in the nucleus at each specific time point ± S.E.M. n=3. Statistical analysis comparing FLAG or VAPB-WT to VAPB-P56S expressing cells were performed using a Student t-test, $p<0.05$*. Scale bar, 10µm.

VAPB Knockdown with siVAPB Demonstrates a Delay in the Nuclear Entry of GR

It was crucial to assess if knocking down endogenous VAPB displays similar delays in nuclear translocation of activated GR as does VAPB-P56S. HeLa cells were co-transfected with GFP-tagged GR and with either pLKO.1 empty control or siVAPB. Nuclear fluorescence was quantified as a percentage of total cellular fluorescence, as previously described.

GR was localized to the nucleus at 15 min in 68% ± 9% (n=3) of empty pLKO.1 transfected cells (Fig. 25A and C). In contrast, nuclear localization of GR-GFP was significantly lowered in knockdown of endogenous VAPB transfected cells with only 29% ± 8.5% of transfected cells exhibiting nuclear GR-GFP at 15 min (Fig. 25B and C). At 30 min, 80% ± 2.1% of pLKO.1 cells displayed nuclear GR-GFP compared to 51% ± 5.9% in shVAPB cells. At 45 min, pLKO.1 cells showed 85% ± 2.5% of nuclear GR signal and shVAPB was still significantly lower with only 63% ± 5.1% of cells with a nuclear localization of GR. GR-GFP was eventually translocated to the nucleus at 60 min in shVAPB transfected cells at a level comparable to the pLKO.1 control group (Fig. 25A, B and C). Thus, upon knockdown of endogenous VAPB which causes a NE defect, there is a significant delay in nuclear translocation.

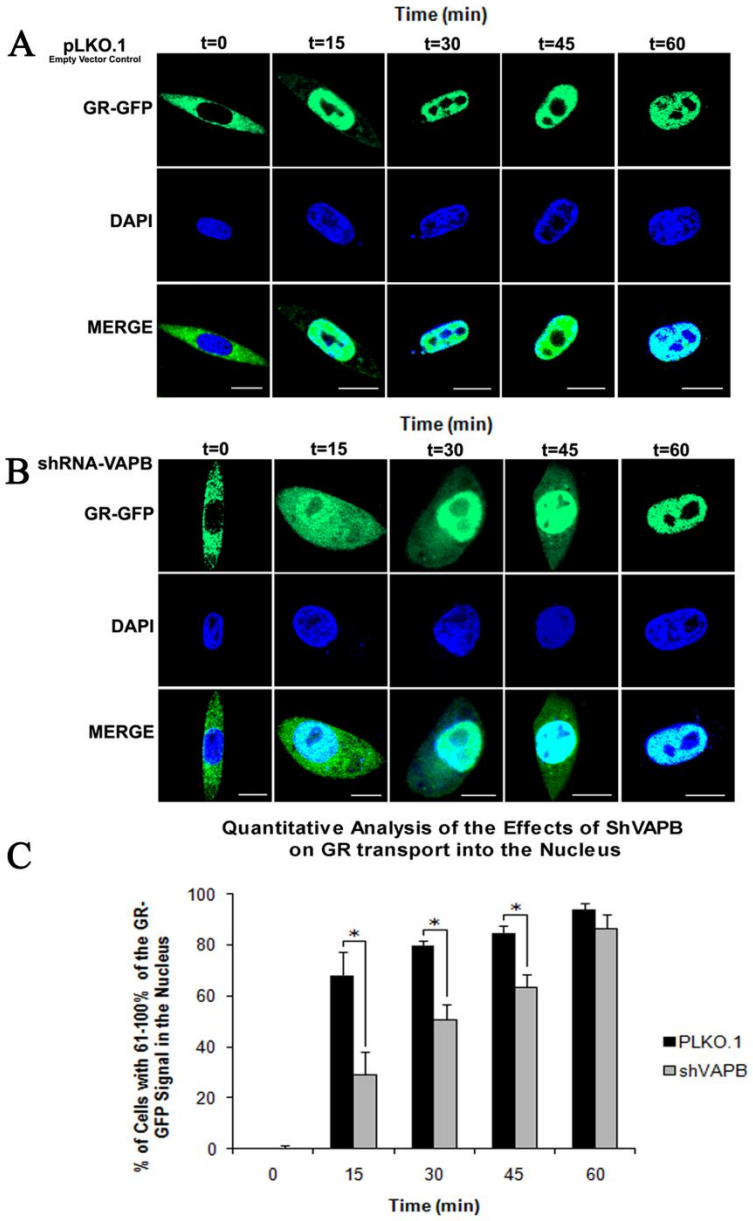

Figure 25. Knockdown of endogenous VAPB causes a time delay in nuclear translocation of activated GR. HeLa cells were co-transfected with pLKO.1 empty vector (A) or shVAPB (B) and GR-GFP. Forty eight hours after transfection, 1 µm of dexamethasone was administered and cells were fixed and mounted with DAPI every 15 minutes for one hour. (C) An average of 65 cells was quantified for each condition. Values are represented as % HeLa cells containing 61-100% of the GR-GFP signal in the nucleus at each specific time point ± S.E.M., n=3. Statistical analysis comparing pLKO.1 + GR-GFP to shVAPB + GR-GP expressing cells were performed using a Student t-test, $p<0.05$*. Scale bar, 10µm.

VAPB Knockdown with shVAPB Increase GR Nuclear Translocation Time

Empty FLAG and VAPB-WT transfected cells exhibited nuclear GR in 15 minutes after Dex administration. In contrast, nuclear localization of GR-GFP was delayed in VAPB-P56S transfected cells. This suggests that VAPB-P56S-induced changes in the NE are the likely cause of the delay. GR was localized to the nucleus at 15 min in empty pLKO.1 transfected cells whereas nuclear localization of GR-GFP was significantly lowered in VAPB knockdown transfected cells. Thus, upon VAPB knockdown, there was also a significant delay in nuclear translocation. In order to visualize the nuclear translocation of GR and to eliminate any possible artifacts due to fixing and staining cells, I utilized a live-imaging technique. Cells were transfected with GR-GFP and either pLKO.1 or siVAPB and maintained as previously described; however, cells were imaged live.

Upon imaging six cells for each condition, I quantified the effects of endogenous VAPB knockdown on GR nuclear transport. The findings show a significant difference between the groups from 5-38 minutes. pLKO.1 transfected cells exhibit a steep slope, indicating a faster rate in nuclear translocation. In addition, cells had ≥60% of GR in the nucleus by ~10 min (Fig. 26). In contrast, cells transfected with shVAPB display a more gradual incline of GR nuclear entry. Knockdown cells exhibited ≥60% of GR in the nucleus by ~35-40 min (Fig. 26).

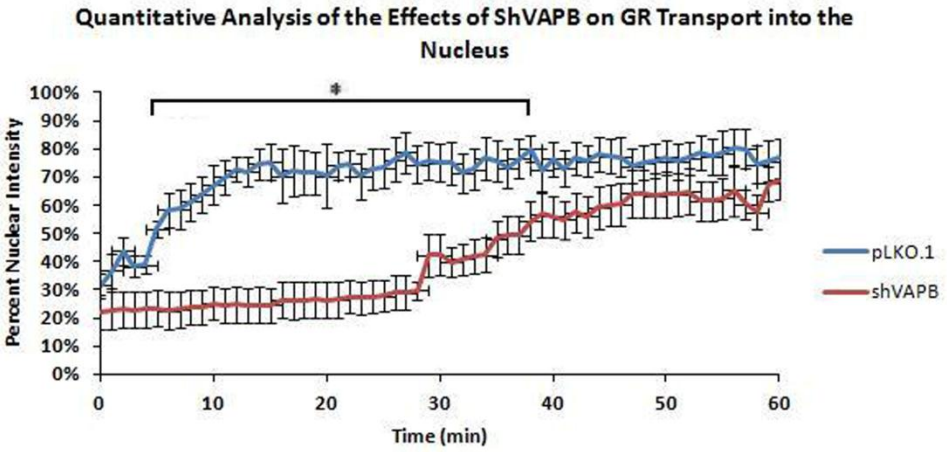

Figure 26. Knockdown of endogenous VAPB increase nuclear translocation time of GR. HeLa cells were co-transfected with GR-GFP and either pLKO.1 or shVAPB. Forty-eight hours later, 1μM Dexamethasone was administered in serum free media and then the cells were imaged live on a Zeiss LSM510 Meta laser scanning confocal microscope for 1 hour. Values are represented as % of GR-GFP signal in the nucleus at each specific time point ± S.E.M., n=6 for each condition. Statistical analysis comparing pLKO.1 to shVAPB expressing cells were performed using a Student t-test, $p<0.05$*.

Addressing the biophysical properties of the P56S mutation in VAPB

FFAT Changes the Solubility Properties of VAPB-P56S

It has been shown that overexpression of FFAT resolves the large ER aggregates and the inhibitory effect of VAPB-P56S on vesicular transport between the ER and the Golgi (Prosser et al., 2008). However, it remains unclear how overexpression of the FFAT motif resolves the aggregation and inhibition. The solubility features of VAPB-WT and VAPB-P56S have been previously examined (Kanekura et al., 2006; Moumen et al., 2011). It was found that the VAPB-WT protein is soluble in Triton X-100. In contrast, VAPB-P56S is insoluble in Triton X-100 and soluble in SDS (Kanekura et al., 2006; Moumen et al., 2011). Thus I examined if the FFAT motif may alter the biophysical properties of VAPB-P56S.

The collection of cell lysates was performed as did the Moumen group and as outlined in the methods and materials section of this thesis. Once the Triton-X-100 and SDS fractions were collected I underwent basic western blot procedure. VAPB-WT was found to be Triton-X-100 soluble while VAPB-P56S was not soluble in Triton-X-100 and found in the SDS fraction. Co-expression of FFAT had no effect on VAPB-WT solubility but rendered mutant VAPB Triton-X-100 soluble (Fig. 27). Co-expression of AAAT unexpectedly shifted some VAPB-WT to the insoluble fraction and AAAT had no effect on mutant VAPB. Interestingly, the FFAT motif was able to shift VAPB-P56S from the SDS fraction to Triton X-100 fraction (Fig. 27) altering the biophysical properties of the VAPB mutant protein. Thus, FFAT may relive the adverse effects of the P56S mutation by altering is solubility properties.

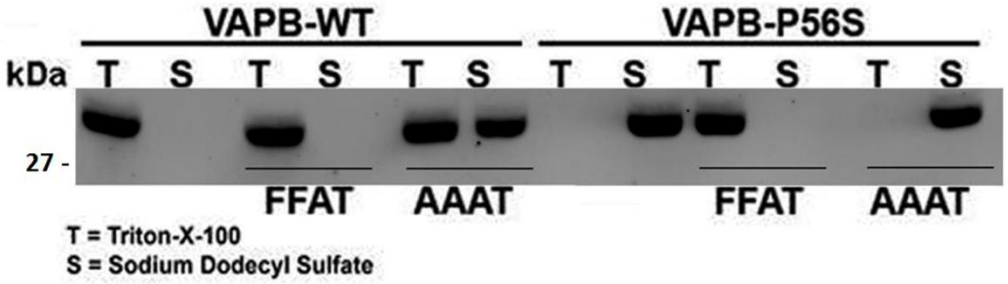

Figure 27. The effect of the FFAT motif on the solubility of VAPB-P56S. HeLa cells were transfected with either VAPB-WT, VAPB-WT+FFAT, VAPB-WT+AAAT, VAPB-P56S, VAPB-P56S+FFAT or VAPB-P56S +AAAT vectors following differential detergent extraction. Anti-FLAG was used to stain for Flagged Tagged VAPB followed by alexa-488 (green) following basic Western Blot procedures.

DISCUSSION

Characterizing the Functional Role of VAPB in Transport of INM and NPC Proteins

Gp210, Nup214, and Emerin are mis-localized in VAPB-P56S Transfected Cells

The current study follows the discovery that overexpression of VAPB-P56S results in the separation of the INM and ONM of the NE (Tran et al., 2012). EM images of CHO cells transfected with VAPB-P56S show enlarged ER structures and a nucleus with areas of separation between the ONM and INM of the NE (see Fig. 5). This led me to believe there is a NE defect and suggests there may be a defect in the transport of proteins required for proper NPC assembly. Since the NPC structurally contributes to the NE bilayers close apposition, deterioration in NPC assembly and recruitment of proteins can ultimately lead to the separation and dilation of the NE bilayers. This suggests that the mechanism responsible for the loss of motor neurons could be due to defects at the NE.

EM images revealed that overexpression of VAPB-P56S, among its other functional deficits, induces a change in the structure of the NE resulting in the separation of the INM and ONM. This separation could be the result of the mis-localization of proteins in the nuclear lamina on the INM or from the transport defects of Nups needed to anchor the NPC to the NE to hold the tight apposition between the lipid bilayers. These questions were examined by employing fluorescent microscopy to test the localization of NPC and NE proteins in VAPB-P56S expressing cells. The findings in this thesis suggest that VAPB is involved in NPC and NE protein transport from the ER to the NE and the FFAT motif can counteract the mutant's adverse effects by restoring proper protein localization. Gp210 has been proposed to play a role in fusing the ONM and INM at the pore. To date, Gp210, Pom121 and Ndc1 are the three integral membrane proteins of the NPC which anchor the NPC to the NE (Antonin et al., 2005). Gp210 is a type 1 integral protein of the NPC with a single membrane spanning region close to the C-terminus of

the protein (Antonin et al., 2005). This study showed that in VAPB-WT expressing cells Gp210 forms a ring-like pattern encompassing the rim of the NE as well as localized to scattered puncta (see Fig. 6A). In contrast, Gp210 was excluded from the NE and retained in mutant VAPB dilated membranes in the cytoplasm (Fig. 6A). These results are consistent with the claims that a defect in nuclear envelope has been reported in sporadic ALS cases (Kinoshita et al., 2009). The loss of the integral membrane protein of the NPC, Gp210, may result in the dilation of the NE and be manifested by irregular nuclear contours.

The separation of the INM and ONM and the expansion of ER tubules in mutant VAPB expressing cells could affect insertion of NPCs leading to a decrease in the number of NPCs on the NE. The loss of NPC from the NE could result in the specific death of non-dividing cells such as motor neurons in ALS8. Hetzer's group examined the rejuvenation of NPC proteins and their study proposed that in non-dividing cells the scaffold nucleoporins (Nups) which make up the nuclear pore are downregulated and do not renew (D'Angelo et al., 2009). On the other hand, peripheral Nups can be exchanged in time (D'Angelo et al., 2009). This implies that the vitality of Nups localized to the scaffold of the nuclear pore is crucial for the survival and proper function of the NPC. Since scaffold proteins do not renew, they are more prone to oxidative damage (D'Angelo et al., 2009). This can result in the loss of the specific permeability of the NE and can induce cytoplasmic proteins to leak into the nucleus (D'Angelo et al., 2009). If this mechanism leads to cell death in ALS8 due to the loss of NPC integrity then the leakiness of the nucleus can result in a toxic gain of function.

To determine if other Nups are affected upon expressing VAPB-P56S, I examined Nup214, a Nup confined to the cytoplasmic face of the NPC (Xu et al., 2009). In a similar fashion to Gp210, Nup214-GFP was localized to the NE in empty vector and VAPB-WT transfected cells, but

sequestered in mutant VAPB containing aggregates (see Fig 7A). Gp210 and Nup214 are retained in the cytoplasmic foci along with aggregated mutant VAPB, suggesting mutant VAPB inhibits their transport to the NE.

To determine if proteins associated with the architectural and structure support system of the NE are affected, I examined the localization of Emerin and Lamin-b1 in cells overexpressing VAPB-P56S. Lamin-B1 stabilizes the NE and anchors nuclear membrane proteins to the scaffold of the INM (Holaska et al., 2006). Emerin is an integral protein of the INM expressed in almost all human cells (Holaska et al., 2006). Emerin binds to Lamins, anchoring Emerin for architectural, gene regulator and nuclear assembly roles (Holaska et al., 2006). Emerin binds to and co-localizes with A and B-type Lamins in the INM (Holaska et al., 2006). I was able to show that Emerin-GFP forming a ring-like pattern along the rim of the NE in both control and VAPB-WT overexpressing cells (Fig 8A). In contrast, Emerin was retained in dilated cytoplasmic membranes and excluded from the NE in mutant VAPB overexpressing cells (Fig. 8A). This effect is not cell line specific as this was seen in CHO and HeLa cells. Lamin-B1, however, was not affected by the cytoplasmic aggregates created by overexpressing VAPB-P56S (see Fig. 9). In VAPB-WT and control cells, Lamin-B1 formed a stable ring-like pattern around the NE which was not distorted by mutant VAPB (see Fig. 9). Emerin is retained in the INM in part by binding to Lamins in the nuclear lamina. Thus, Lamin-B1 was examined to address whether Emerin transport was affected or if its retention to the Lamin scaffold was altered causing Emerin to accumulate in the cytoplasm upon overexpression of VAPB-P56S (Vaughan et al., 2001). Examining the distribution of Lamin-B1 showed no change in distribution pattern or evidence of nuclear deformation. Therefore, the loss of Emerin from the INM is likely due to disruption of transport to the INM rather than loss of retention at the INM.

The loss of NPC proteins and INM proteins suggests that NPC production and insertion into the NE is decreased. In addition, the lack of newly produced scaffold Nups and the lack of transport of newly synthesized peripheral Nups from the ER to the NE in motor neurons in VAPB-P56S expressing cells predicts that these cells would have less NPCs. VAPB-P56S and knockdown of VAPB illustrates that VAPB is vital in the transport of Nups and NE proteins from the ER to the NE. Without VAPB assisted transport, the already inserted NPCs would not be able to synthesize new proteins and with time, age-deterioration of the NPC will make neuronal cells vulnerable to protein damage and cell death (D'Angelo et al., 2009). This can explain the specific target towards motor neurons and the late-onset nature of ALS8.

Leaky nuclear pores could contribute to cell death as suggested by D'Angelo et al. (2009) which showed how aging accelerated the leakiness of the nucleus (D'Angelo et al., 2009). This study examined the effect of oxidative damage and age-related deterioration on NPC. They utilized the environmental toxin Paraquat to induce oxidative damage by increase the amount of reactive oxygen species (ROS) in *Caenorhabditis elegans* for six days (D'Angelo et al., 2009). They found that paraquat treated worms had greater amounts of the 70 kDa dextran in their nucleus compared to controls and dextran is too great a size to transport through an intact NPC. They also showed that the nuclear permeability of older worms was deteriorating compared to younger worms. In addition, this permeability deterioration was accelerated with paraquat treatment (D'Angelo et al., 2009). Age-related deterioration of NPCs leads to the loss of the NPC selective permeability barrier (D'Angelo et al., 2009). Altogether, expression of VAPB-P56S altered NE morphology and NPC composition affecting its permeability and can explain for the preferential vulnerability of motor neurons to premature death and the late-onset of ALS8.

The FFAT Motif Rescues Mis-Localized NE and NPC Proteins of VAPB-P56S

The simultaneous overexpression of the FFAT-motif with mutant VAPB resolved the abnormal ER morphology and restored ER-Golgi trafficking (Prosser et al., 2008). Thus, I addressed whether this could resolve the effects of the mutation on Nups and NE proteins. The formation of the ER expanded tubules that trapped Gp210, Nup214 and Emerin may be the result of increased lipid synthesis at the ER (Prosser et al., 2008). Increased lipid synthesis recruits endogenous FFAT-motif-containing lipid proteins to the ER by VAPB-P56S which increased the interaction of these FFAT containing proteins with the MSP domain of VAPB. Increased interaction with no proper regulation of lipids at the ER can induce theses expanded ER tubules seen in cells overexpressing VAPB-P56S (Prosser et al., 2008). This rationale is based on studies illustrating the interaction between the MSP domain of VAP with the FFAT motif of lipid-binding proteins (Loewen and Levine, 2005). The role of this interaction is to maintain and regulate lipids at the ER (Wyles et al., 2002). Studies have shown that VAPB-P56S does not hinder FFAT binding to the MSP domain of SCS2, the yeast orthologue of VAP. SCS2-P51S, a mutation that manifests itself like P56S in human VAPB, is able to interact with the FFAT motif of Opi1p (Loewen and Levine, 2005). Thus, since VAPB-P56S can interact with FFAT containing proteins and this interaction may be increased, the lipid composition at the ER may not be properly regulated. Upon co-transfection of the FFAT motif with VAPB-P56S the adverse effects of mutant VAPB are resolved. This suggests that exogenous expression of the FFAT motif may outcompete endogenous FFAT-containing lipids and therefore restore proper lipid composition of the ER by reducing the amount of FFAT-motif containing lipid proteins interacting with VAPB at the ER. Normal nuclear localization of both Gp210-GFP and Nup214-GFP were restored upon co-overexpression of the FFAT fragment with VAPB-P56S (see Fig. 6B and Fig 7B, respectively). Co-overexpression of FFAT also restored Emerin localization to the NE in mutant VAPB co-

overexpressing cells (see Fig. 8B). Thus, the FFAT motif can resolve the formation of VAPB-induced aggregates and relieve the transport defect of these Nups and Emerin. This may suggest that, exogenous FFAT motifs binds to the MSP domain of VAPB-P56S and outcompetes endogenous FFAT motif-containing lipid proteins.

Altogether, overexpression of VAPB-P56S expanded ER tubules and blocked transport of Nups and INM proteins suggesting that VAPB-P56S alters ER protein trafficking. Co-expression of the FFAT motif resolved ER tubule expansion and corrected the localization of NPC and NE proteins to the NE. The alteration in NE morphology induced by VAPB-P56S has not been documented in previous studies, and suggested that VAPB-P56S alters functions associated with the NE and NPC.

Emerin, Pom-121, and Nup-214 are Mis-Localized upon siVAPB Knockdown

Mutant VAPB is prone to aggregates and can recruit endogenous VAPB to insoluble aggregates resulting in a dominant negative effect (Teuling et al., 2007). To determine whether transport defect is due to loss of VAPB function and to exclude non-specific sequestration of NE proteins with aggregated mutant VAPB, I examined the distribution of Emerin, Pom121 and Nup214 upon siRNA knockdown of endogenous VAPB. Since similar phenotypes were observed in siRNA cells as in overexpressing VAPB-P56S, this suggests that the P56S mutation causes a loss of endogenous VAPB function.

Knockdown of endogenous VAPB with siVAPB caused Nup214-GFP to relocate to the cytoplasm and was lost from the NE (see Fig. 10A). Transport of Emerin was similarly inhibited by knockdown of VAPB with endogenous Emerin relocated from the NE to large cytoplasmic puncta throughout the cell (see Fig. 10B). In addition, Pom121-GFP was also excluded from the NE and

retained in large cytoplasmic puncta upon siVAPB (see Fig. 10C). This demonstrates that VAPB is essential for transport of these Nups. Altogether, the accumulation of Nup214-GFP, Pom121-GFP and Emerin in siVAPB suggests that VAPB function is required for transport of pre-assembled NPC to the NE. This is consistent with the view that mutant VAPB acts in a dominant negative manner. Loss of NE protein localization is not simply due to inadvertent sequestration of Nups with protein aggregates but likely a consequence of loss of endogenous VAPB in mutant VAPB overexpressing cells. Thus, VAPB clearly plays an essential role in Nup and NE protein's transport to the NE.

Characterizing the Compartment in which INM and NPC Proteins are Retained

VAPB is Localized to the ERGIC

VAPA and VAPB have been implicated in intracellular trafficking of cargo proteins. The major objective of this study is to characterize if VAPB plays a role in the transport of NPC and NE proteins. My previous results have suggested that VAPB-P56S induces expanded ER tubules that block the transport of Gp210 and Nup214 to the NPC. Also, VAPB-P56S interferes with the transport of Emerin to the INM. The results indicate that these proteins are not sequestered into VAPB-P56S-induced aggregates; however, they are retained in the cytoplasm due to loss of VAPB function. This loss of VAPB function was illustrated through knocking down the synthesis of VAPB with siRNA. In order to clarify where Nups and INM proteins are retained in the cytoplasm I examined compartments of the early secretory pathway that hold both anterograde and retrograde transport routes. Dr. Ngsee and Wendy Zhang showed that anterograde ER-to-Golgi transport of VSVG is unaffected upon siVAPB knockdown (Tran et al., 2012). This suggests that VAPB does not regulate anterograde transport of proteins from the ER. Thus, in order to determine the compartment in which Nups and NE proteins are retained in and to identify if this

compartment contains VAPB, I examined an organelle that displays retrograde movement: The Endoplasmic Reticulum Golgi Intermediate Compartment (ERGIC). Firstly, I addressed if this compartment contains VAPB. The results suggest that VAPB-WT co-localized extensively with ERGIC-53-GFP cytoplasmic puncta (see Fig. 11) and the Golgi ribbons lacked VAPB (see Fig. 12) indicating that VAPB resides primarily at the ERGIC. Intensity correlation analysis showed that VAPB co-localizes with the ERGIC suggesting that VAPB may function in retrograde transport of proteins from the ERGIC to the ER or the NE.

VAPB-P56S and siVAPB Compromises the ERGIC

To further understand the effects of VAPB on the ERGIC, VAPB-P56S and siVAPB were expressed in cells with ERGIC-53-GFP. Both VAPB-P56S expression and knocking down endogenous VAPB resulted in expanded ERGIC membranes with a greater diameter compared to control cells. Cells transfected with either VAPB-P56S or shVAPB exhibit an expansion in the diameter of the ERGIC. The results indicated that the expansions of the ERGIC may be due to the accumulation of cargo at the ERGIC that is not transported due to loss of VAPB-assisted retrograde transport.

Emerin, Mab414 and Nup214-RFP Correlate with the ERGIC and are Retained at the ERGIC upon shVAPB

The previous results indicated that VAPB co-localizes with the ERGIC and the ERGIC is expanded upon overexpression of VAPB-P56S and siRNA knockdown of endogenous VAPB. From this I inferred that the expansion may be due to an accumulation of proteins transported to the ERGIC and then are retained at the ERGIC in the absence of VAPB. Thus, VAPB is likely to function in the retrograde transport of proteins from the ERGIC.

Emerin, Nup214 and Mab414 were tested to see if they co-localized with expanded ERGIC

membranes. Emerin, Nup214 and Mab414 staining showed an increase in both Pearson's correlation and Mander's overlap coefficient when subjected to VAPB-P56S or knockdown of VAPB compared to VAPB-WT or controls. These figures support the hypothesis that NE proteins and Nups transit through the ERGIC via vesicular transport prior to the NE. In addition, the cytoplasmic aggregates were extremely expanded in diameter indicating that Nups and NE proteins transported to the ERGIC were retained at the ERGIC in a VAPB-dependent manner. These proteins were seen to be relocated from the NE to the ERGIC-expanded membranes in VAPB-P56S overexpressing cells and siVAPB. These results support the view that NE proteins and Nups transit through the ERGIC and VAPB plays a role in the retrograde trafficking of these proteins from the ERGIC to the NE. This is consistent with an earlier study on VAPB by Elazar's group. They demonstrated that addition of antibodies against ERG30 (now known as VAPB) accumulated COPI-coated vesicles. COPI-coated vesicles transport retrograde cargo from the Golgi complex to the ER (Soussan et al., 1999). Altogether, this indicates that NE proteins and Nups transit through the ERGIC and VAPB is required for final transport to the NE.

Lateral Diffusion or Vesicular Transport

Cytoplasmic retention of Nups and Emerin in mutant VAPB aggregates is not due to inadvertent sequestration with insoluble aggregates since siRNA knockdown of endogenous VAPB also results in their cytoplasmic retention. Transport of Nups and INM proteins have been proposed to be targeted to the NE through lateral diffusion along the ER membrane and the NE due to the connection between the ER and the ONM (Ostlund et al., 1999).However, given that VAP-WT resides primarily at the ERGIC and siVAPB knockdown results in expansion of the ERGIC and retention of Nup and Emerin at the ERGIC, I suggests that these NE membrane proteins do not reach the NE by lateral diffusion through the interconnecting ER and ONM network, but transit

through ERGIC by vesicular transport. Once the proteins reach the ERGIC they are then transported to the NE. Transport from these ERGIC foci is clearly dependent on VAPB. However, with loss of function either through siRNA knockdown or the dominant negative effect of mutant VAPB overexpression, inhibiting proteins from exiting the ERGIC causes the ERGIC to expand. While the mechanism by which VAPB facilitates this retrograde transport step remains to be determined, deterioration of the NE and NPC is a consequence of disrupting this transport step and may contribute to age-dependent onset of the disease.

Nup214 – A Soluble Protein Synthesized in the Cytosol

Studies are trying to address how and where the NPCs are assembled. There are two models that propose how NPCs are assembled. According to the insertion model, presence of the NE is required for the assembly of the NPC because after NPCs are formed they are inserted into the NE (Lu et al., 2011). In the pre-pore model, Nups are recruited to the chromatin and then assemble into substructures on regions devoid of NE and then the remaining Nups are recruited after the NE forms (Lu et al., 2011). Although I did not test either model, the obtained results may be helpful in addressing where NPCs are assembled. Nup214 is a soluble protein synthesized in the cytosol and this site of production gives Nup214 the ability to be recruited to the NE immediately after synthesis. However, my results indicated this is not the case. I showed that Nup214 shows a high Pearson's correlation with the ERGIC. In addition, Nup214 is retained in the VAPB-P56S and siVAPB-induced expanded ERGIC in a similar fashion to Mab414 and Emerin. Thus, Nup214 is recruited to the ERGIC with other Nups prior to transport to the NE. I suggest that NPCs may be partially assembled at the ERGIC prior to transport to the NE. According to the two models of NPC assembly, the results obtained may support the insertion model which suggests that NPCs are assembled in the presence of an existing NE. CHO cells and

HeLa cells with intact NE were examined and Nup214 along with Gp210 was synthesized. Thus, it may be possible that NPCs are assembled at the ERGIC and then transported to the NE for their insertion into the NE.

Consequence of a Defected NE and NPC assembly

One of the characteristics of SALS and FALS is the mislocalization of the nuclear protein TAR-DNA-binding protein-43 (TDP-43) to the cytoplasm (Anagnostou et al., 2008). A recent study demonstrated that transgenic mice expressing human VAPB-P56S in the brain and spinal cord regions of the nervous system showed TDP-43 localized in the cytoplasm as early as 18 months of age (Tudor et al., 2010). TDP-43 localized in the cytoplasm instead of the nucleus suggests there is a functional defect in the permeability of the NE. The previous results from this thesis suggest that NPC and NE proteins are not properly transported to the NE and are retained at the ERGIC due to the loss of VAPB retrograde transport. The loss of proper NPC and NE protein transport may induce a leaky nucleus which may explain TDP-43 redistribution. Nucleocytoplasmic shuttling is crucial in establishing cellular function and cell viability (Zhang, et al., 2006). Since TDP-43 is mis-localized, a dysfunction in nucleocytoplasmic shuttling may be the consequence of a defect in NPC assembly in ALS8.

Through utilizing the ligand-activated glucocorticoid receptor, I showed that an altered NPC composition induced by VAPB-P56S overexpression had an effect on nucleocytoplasmic shuttling. Upon Dex administration, the activated GR-GFP translocated into the nucleus within 15 minutes in VAPB-WT cells (see Fig. 23A and C). In contrast, nuclear localization of GR-GFP was significantly delayed in VAPB-P56S overexpressing cells with GR-GFP nuclear translocation at 45 and 60 min intervals. This suggests that nuclear import was significantly delayed but not completely blocked in VAPB-P56S overexpressing cells (see Fig. 23B and C). Simultaneous

overexpression of FFAT with mutant VAPB restored the import delay (see Fig. 24 A, B and C); suggesting mutant VAPB-induced changes are the likely cause of the delay. Further, knocking down the synthesis of VAPB also delayed the nuclear translocation of activated GR-GFP up to 60 min compared to empty pLKO.1 transfected cells exhibiting nuclear GR tranloscation at 15 min (see Fig. 25A, B and C). These results suggest that upon knockdown of endogenous VAPB a defect in NE structure and NPC composition is induced. Subsequently, the rate of nucleocytoplasmic shuttling maybe significantly reduced due to a reduction in the amount of functional NPCs at the NE. These results may suggest that TDP-43 is redistributed from the nucleus and GR-GFP is delayed entry into the nucleus because of a deficit in NE and NPC assembly.

Kusaka's group investigated the nucleocytoplasmic transport system in ALS (Zhang et al., 2006). Their results support my results that activated GR is delayed in entry to the nucleus in VAPB-P56S cells and in knockdown of VAPB expressing cells. This delay could be caused in ALS8 by disruption of the insertion of functional NPCs into the NE causing activated GR to be delayed in the cytoplasm.

Initially, it was thought that the delay in nuclear GR translocation could be cause by the mis-targeting of activated GR to pre-assembled NPC retained in the ERGIC expanded membranes. In the current thesis cytoplasmic accumulation of activated GR-GFP was visualized in mutant VAPB transfected cells at 15 and 30 min time intervals. Empty vector and VAPB-WT co-transfected cells showed GR nuclear fluorescence 15 min after Dex treatment. Cells with GR aggregates lacked a nuclear signal, suggesting that GR was mis-targeted. In order to test if the GR aggregates observed is due to the recruitment of activated GR-GFP to Nups retained in the mutant VAPB-induced dilated ERGIC membranes, antibodies towards Nups containing FG

repeats, for instance Mab414, in VAPB-P56S transfected cells should be examined at 15 min and 30 min after Dex treatment. If the distribution of GR and Mab414 co-localized then it may be plausible that GR is mis-targeted to pre-assembled Nups in the cytoplasm. However, through examination in this current thesis no co-localization of Nups with GR-GFP aggregates in the cytoplasm was seen. Further, previously I assumed the aggregates formed by the VAP-P56S mutation recruits GR into these aggregates. However, this is not likely the case because knockdown of endogenous VAPB induces a time delay without the formation of aggregates.

Lastly, I propose that the time delay could be due to a lower density of properly assembled and inserted NPC in the NE. The widening of the perinuclear space caused by the separation of the ONM and INM and the loss of surface area on the nucleus could affect insertion of NPCs leading to a decrease in NPCs on the NE. NPC consists of approximately 2-3000 pores. VAPB-P56S and shVAPB may reduce the number of functional pores at the NE, thus resulting in a time delay in nuclear translocation. As the cell ages, the disease progresses and degeneration becomes extremely evident. Subsequently, the cells may die due to loss of proper NPC activity. This effect could explain the vulnerability in non-dividing cells such as motor neurons. From my results, it is clear there is a compromise in the transport of NPC proteins and in the assembly of NPCs. Therefore, I propose this is a likely mechanism for the time delay in nuclear translocation of activated GR. This alteration in the distribution of NPCs influences nucleocytoplasmic shuttling and may be a leading cause of pathogenesis in ALS8.

Addressing the Biophysical Properties of the P56S Mutation in VAPB

The simultaneous over-expression of the FFAT-motif with mutant VAPB resolves the abnormal ER morphology and restores ER-Golgi trafficking (Prosser et al., 2008). Co-overexpression of the FFAT fragment counteracts the effects of mutant VAPB and interferes with mutant VAPB aggregate formation (Prosser et al., 2008). The current thesis showed that the FFAT-motif resolves the effects of the mutation on Nups and NE proteins. The normal localization of both Gp210 and Nup214 were restored upon co-overexpression of the FFAT fragment with VAPB-P56S (see Fig. 6B and Fig 7B, respectively). Co-overexpressoin of FFAT and VAPB-P56S also restored Emerin to the NE (see Fig. 8B). The FFAT motif also restored nuclear translocation of activated GR-GFP in VAPB-P56S overexpressing cells. Thus, the FFAT motif resolves the formation of VAPB-P56S aggregates and relieves the transport defect of Nups and NE proteins.

Raoul's group examined the solubility properties of VAPB-WT and VAPB-P56S through differential detergent extraction followed by western blotting (Moumen, et al., 2011). VAPB-P56S resulted in dense and insoluble cytosolic VAPB aggregates (Kanekura et al., 2006; Moumen, et al., 2011). VAPB-P56S was only found in the SDS-soluble fractions whereas the WT protein was found only in the Triton-X 100 fraction (Moumen, et al., 2011). Consistently, this thesis observed the same results. In order to examine if the FFAT motif has an influence on the solubility properties of the mutant VAPB protein, HeLa cells were co-transfected with the FFAT motif and differential detergent extraction was performed. Strikingly, the results obtained showed that co-overexpression of VAPB-P56S and the FFAT motif were found in the Triton-X soluble fraction (see Fig. 27). How the FFAT motif relieves the defects of VAPB-P56S is currently debatable. It is known that VAPB-P56S does not directly affect the binding of FFAT (Loewen and Levine, 2005). VAPB-P56S also does not cause a complete loss of function of the VAPB protein

(Chai et al., 2008). It has been suggested that FFAT binding may induce a conformational changes that reduces mutant VAPB aggregate formation and may restore wild-type function (Tran et al., 2012). My results indicate that binding of the FFAT motif to VAPB-P56S may induce a conformational change in VAPB-P56S resulting in its solubility in the Triton-X-100 fraction similar to the properties of the VAPB-WT protein. This conformational change may restore VAPB function. Inducing this change in the proteins solubility properties may explain why the simultaneous over-expression of the FFAT-motif with mutant VAPB resolves the abnormal ER morphology and restores the trafficking deficits of NPC and NE proteins.

REFERENCES

Amarilio, R., Ramachandra, S., Sabanay, H. and Lev, S. (2005). Differential regulation of endoplasmic reticulum structure through VAP-Nir protein interaction. *J. Biol. Chem.* 280:5934-5944.

Anagnostou, G., Akbar, M. T., Paul, P., Angelinetta, C., Steiner, T. J. and de belleroche, J. (2008). Vesicle associated membrane protein B (VAPB) is decreased in ALS spinal cord. *Neurobiol Aging.*

Antonin, W., Franz, C., Haselmann, U., Antony, C., Mattaj, I. W. (2005). The Integral Membrane Nucleoporin pom121 Functionally Links Nuclear Pore Complex Assembly and Nuclear Envelope Formation. *Mol. Cell.* 17:83-92.

Baker, A.M.E., Roberts, T.M., and Stewart, M. (2002). 2.6 Å resolution crystal structure of helices of the motile major sperm protein (MSP) of *Caenorhabditis elegans*. *J. Mol. Biol.* 319:491-499.

Ben-Tekaya H, Miura K, Pepperkok R, Hauri HP (2005) Live imaging of bidirectional traffic from the ERGIC. *J. Cell Sci.* 118(Pt 2):357-367

Boillee, S., Vande Velde, C. and Cleveland, D.W. (2006). ALS: a disease of motor neurons and their nonneuronal neighbors. *Neuron* 52:39-59

Brickner, J.H., and P. Walter. 2004. Gene recruitment of the activated INO1 locus to the nuclear membrane. *PLoS Biol.* 2:e342.

Burke, B. and Stewart, C.L. 2006. The laminopathies: the functional architecture of the nucleus and its contribution to disease. *Annu Rev Genomics Hum Genet* 7:369-405.

Chai, A., Withers, J., Koh, Y. H., Parry, K., Bao, H., Zhang, B., Budnik, V. and Pennetta, G. (2008). hVAPB, the causative gene of a heterogeneous group of motor neuron diseases in humans, is functionally interchangeable with its Drosophila homologue DVAP-33A at the neuromuscular junction. *Hum. Mol. Genet.* 17, 266-280.

Cozzolino, M., Ferri, A. And Carri, M.T. (2008). Amyotrophic lateral sclerosis: from current developments in the laboratory to clinical implications. *Antioxid Redox Signal* 10:405-443.

D'Angelo, M.A., Raices, M., Panowski, S.H. and Hetzer, M.W. (2009). Age-dependent deterioration of nuclear pore complexes causes a loss of nuclear integrity in postmitotic cells. *Cell* 136:284-295.

Hamamoto, L., Nishimura, Y., Okamoto, T., Aizaki, H., Liu, M., Mori, Y., Abe, T., Suzuki, T., Lai, M. M., Miyamura, T. et al. (2005). Human VAP-B is involved in hepatitis C virus replication through interaction with NS5A and NS5B. *J. Virol* 79:13473-13482.

Hauri HP, Kappeler F, Andersson H, Appenzeller C. (2000) ERGIC-53 and traffic in the secretory pathway. *J. Cell Sci.* 113(Pt 4):587-596

Holaska, J. M., Wilson, K. L. (2006). Multiple roles for emerin: implications for Emery-Dreifuss muscular dystrophy. *Anat Rec A Discov Mol Cell Evol Biol.* 288(7):676-680.

Kaiser, S.E., Brickner, J.H., Reilein, A.R., Fenn, T.D., Walter, P. and Brunger, A.T. (2005). Structural basis of FFAT motif-mediated ER targeting. *Structure* 13:1035-1045.

Kanekura, K., Nishimoto, I., Aiso, S. and Matsuoka, M. (2006). Characterization of amyotrophic lateral sclerosis-linked P56S mutation of vesicle-associated membrane protein-associated protein B (VAPB/ALS8). *J. Biol. Chem.* 281 :30223-30233.

Kanekura, K., Suzuki, H., Aiso, S. and Matsuoka, M. (2009). ER stress and unfolded protein response in amyotrophic lateral sclerosis. *Mol Neurobiol.* 39:81-89.

Kinoshita Y, Ito H, Hirano A, Fujita K, Wate R, Nakamura M, Kaneko S, Nakano S, Kusaka H (2009) Nuclear contour irregularity and abnormal transporter protein distribution in anterior horn cells in amyotrophic lateral sclerosis. *J Neuropathol Exp Neurol* 68:1184-1192.

Kukihara, H., Moriishi, K., Taguwa, S., Tani, H., Abe, T., Mori, Y., Suzuki, T., Fukuhara, T., Taketomi, A., Maehara, Y. et al. (2009). Human VAP-C negatively regulates hepatitis C virus propagation. *J. Virol.* 83:7959-7969.

Lev, S., Ben Halevy, D., Peretti, D. and Dahan, N. (2008). The VAP protein family: from cellular functions to motor neuron disease. *Trends Cell Biol.* 18:282-290.

Loewen, C. J. and Levine, T. P. (2005). A highly conserved binding site in vesicle-associated membrane protein-associated protein (VAP) for the FFAT motif of lipid-binding proteins. *J. Biol. Chem.* 280:14097-14104.

Loewen, C. J., Roy, A. and Levine, T. P. (2003). A conserved ER targeting motif in three families of lipid binding proteins and in Opi1p binds VAP. *EMBO J.* 22:2025-2035.

Lu L, Ladinsky MS, Kirchhausen T (2011) Formation of the postmitotic nuclear envelope from extended ER cisternae precedes nuclear pore assembly. *J Cell Biol* 194(3):425-440.

Moumen A, Virard I, Raoul C (2011) Accumulation of wildtype and ALS-linked mutated VAPB impairs activity of the proteasome. *PLoS One* 6(10):e26066

Meyer, J. S., Quenzer, L. F. (2005). Psychopharmacology : Drugs, the Brain, and Behavior. Sinauer Associates Inc. Sunderland, Massachusetts USA.

Nishimura, Y., Hayashi, M., Inada, H. and Tanaka, T. (1999). Molecular cloning and characterization of mammalian homologues of vesicle-associated membrane protein-associated (VAMP-associated) proteins. *Biochem Biophys Res. Commun.* 254:21-26.

Nishimura, A.L., Mitne-Neto, M., Silva, H. C., Richieri-Costa, A., Middleton, S., Cascio, D., Kok, F., Oliveira, J. R., Gillingwater, T., Webb, J. et al. (2004). A mutation in the vesicle-trafficking protein VAPB causes late-onset spinal muscular atrophy and amyotrophic lateral sclerosis. *Am. J. Hum. Genet.* 75:822-831.

Nishimura, A. L., Al-Chalabi, A. and Zatz, M. (2005). A common founder for amyotrophic lateral sclerosis type 8 (ALS8) in the Brazilian population. *Hum. Genet.* 118:499-500.

Olkkonen, V. M. and Levine, T. P. (2004). Oxysterol binding proteins: in more than one place at one time? *Biochem. Cell Biol.* 82:87-98.

Olkkonen, V. M., Johansson, M., Suchanek, M., Yan, D., Hynynen, R., Ehnholm, C., Jauhiainen, M., Thiele, C. and Lehto, M. (2006). The OSBP-related proteins (ORPs): global sterol sensors for co-ordination of cellular lipid metabolism, membrane trafficking and signaling processes? *Biochem. Soc. Trans.* 34:389-391.

Ostlund, C., Ellenberg, J., Hallberg, E., Lippincott-Schwartz, J., and Worman, H. J. (1999). Intracellular trafficking of emerin, the Emery-Dreifuss muscular dystrophy protein. *J. Cell Sci.* 112:1709-1719.

Perry, R. J. and Ridgway, N. D. (2006). Oxysterol-binding protein and vesicle-associated membrane protein-associated protein are required for sterol-dependent activation of the ceramide transport protein. *Mol. Biol. Cell.* 17:2604-2616.

Prosser, D. C., Tran, D., Gougeon, P.Y., Verly, C. and Ngsee, J.K. (2008). FFAT rescues VAPA-mediated inhibition of ER-to-Golgi transport and VAPB-mediated ER aggregation. *J. Cell Sci.* 121:3052-3061.

Prosser, D. C. (2008). Novel links between protein sorting and cytoskeletal dynamics in the secretory pathway. *ProQuest Dissertions and Theses.*

Shaw, P. J., (2005). Molecular and cellular pathways of neurodegeneration in motor neurone disease. *J. Neurol. Neurosurg. Psychiatry.* 76:1046-1057.

Skehel, P. A., Martin, K. C., Kandel, E. R., Bartsch, D. (1995). A VAMP-binding protein from *Aplysia* required for neurotransmitter release. *Science.* 269:1580-1583.

Skehel, P. A., Fabian-Fine, R. and Kandel, E. R. (2000). Mouse VAP33 is associated with the endoplasmic reticulum and microtubules. *Proc. Natl. Acad. Sci. USA.* 97:1101-1106

Soussan, L., Burakov, D., Daniels, M.P., Toister-Achituv, M., Porat, A., Yarden, Y. and Elazar, Z. (1999). ERG30, a VAP-33-related protein, functions in protein transport mediated by COPI vesicles. *J. Cell. Biol.* 146:301-311.

Stavru F, Nautrup-Pedersen G, Cordes VC, Görlich D (2006) Nuclear pore complex assembly and maintenance in POM121- and gp210-deficient cells. *J Cell Biol* 173(4):477-483

Teuling, E., Ahmed, S., Haasdijk, E., Demmers, J., Steinmetz, M. O., Akhmanova, A., Jaarsma, D. and Hoogenraad, C. C., (2007). Motor neuron disease-associated mutant vesicle membrane protein-associated protein (VAP) B recruits wild-type VAPs into endoplasmic reticulum-derived tubular aggregates. *J. Neurosci.* 27:9801-9815.

Tran, D., Chalhoub, A., Schooley, A., Zhang, W., Ngsee, J. K. (2012). Amyotrophic Lateral Sclerosis Mutant VAPB Causes a Nuclear Envelope Defect. *J. Cell Sci.*

Tsuda, T., S. Munthasser, P.E. Fraser, M.E. Percy, I. Rainero, G. Vaula, L. Pinessi, L. Bergamini, G. Vignocchi, D.R.C. McLachlan, W.G. Tatton, and P. St George-Hyslop. (1994) Analysis of the functional effects of a mutation in SOD1 associated with familial amyotrophic lateral sclerosis. *Neuron.* 13:727-736.

Tudor, E. L., Galtrey, C. M., Perkinton, M.S., Lau, K. F., de Vos, K. J., Mitchell, J.C., Ackerley, S., Hortobagyi, T., Vamos, E., Leigh, P. N. et al. (2010). Amyotrophic lateral sclerosis mutant vesicle-associated membrane protein-associated protein-B transgenic mice develop TAR-DNA-binding protein-43 pathology. *Neuroscience.*

Vaughan, A., M. Alvarez-Reyes, J.M. Bridger, J.L. Broers, F.C. Ramaekers, M. Wehnert, G.E. Morris, W.G.F. Whitfield, and C.J. Hutchison. 2001. Both emerin and lamin C depend on lamin A for localization at the nuclear envelope. *J Cell Sci*. 114:2577-90.

Weir, M. L., Xie, H., Klip, A. and Trimble, W. S. (2001). VAP-A binds promiscuously to both v- and tSNAREs. *Biochem Biophys Res Commun.* 286:616-621.

Wyles, J. P., McMaster, C. R. and Ridgway, N. D. (2002). Vesicle-associated membrane protein-associated protein-A (VAP-A) interacts with the oxysterol-binding protein to modify export from the endoplasmic reticulum. *J.Biol Chem.* 277:29908-29918.

Xu, S., Powers, M. A. (2009). Nuclear Pore Proteins and Cancer. *Seminars in Cell & Developmental Biology*. 20:620-630.

Zhang, J., Ito, H., Wate, R., Ohnishi, S., Nakano, S., Kusaka, H. (2006). Altered distribution of nucleocytoplasmic transport-related proteins in the spinal cord of a mouse model of amyotrophic lateral sclerosis. *Acta Neuropathol.* 112(6):673-680.

Zuleger N, Kelly DA, Richardson AC, Kerr AR, Goldberg MW, Goryachev AB, Schirmer EC (2011) System analysis shows distinct mechanisms and common principles of nuclear protein dynamics. *J. Cell Biol.* 193(1):109-123